Hydrologic Design Standards under Future Climate for Grand Rapids, Michigan

Prepared for

City of Grand Rapids

Prepared by

One Park Drive, Suite 200 • PO Box 14409
Research Triangle Park, NC 27709

June, 2015

This report was prepared by Dr. Jonathan Butcher, P.H. and Tan Zi.

Contents

List of Tables

List of Figures

Acronyms

AEP	Annual Exceedance Probability
AMP	Annual Maximum Precipitation
ARI	Average Recurrence Interval
CDF	Cumulative Distribution Function
CMIP3	Coupled Model Intercomparison Project Round 3
CMIP5	Coupled Model Intercomparison Project Round 5
EQM	Equidistant Quantile Mapping
GCM	Global Climate Model
GEV	Generalized Extreme Value
GPD	Generalized Pareto Distribution
IDF	Intensity Duration Frequency
IPCC	Intergovernmental Panel on Climate Change
MACA	Multivariate Adaptive Constructed Analogs
MAGICC/SCENGEN	Model for the Assessment of Greenhouse-gas Induced Climate Change /Regional Scenario Generator
NOAA	National Oceanic and Atmospheric Administration
POT	Peaks-over-Threshold
QM	Quantile Mapping
RCPs	Representative Concentration Pathways
WMEAC	West Michigan Environmental Action Council

(This page left intentionally blank.)

1 Introduction

A Climate Resiliency Report for Grand Rapids was prepared by the West Michigan Environmental Action Council (WMEAC) in 2013. With support from Grand Valley State University, a modeling analysis was used to forecast annual and seasonal temperature and precipitation changes in Grand Rapids through 2042. The model predicted an increase in the average annual precipitation, primarily during winter and spring conditions, along with an increase in average air temperature. Summer monthly precipitation was estimated to decrease; however, the model produced monthly output only and thus cannot inform on the extent to which maximum storm events (design storms) may change. The recent National Climate Change Assessment summary for the Midwest suggests, however, that "extreme rainfall events and flooding have increased during the last century, and these trends are expected to continue, causing erosion, declining water quality, and negative impacts on transportation, agriculture, human health, and infrastructure" (Pryor et al., 2014). Warming air temperatures imply an increase of atmospheric water vapor content of about 7%/°K, implying a comparable increase in extreme precipitation events (Allan and Soden, 2008). Increases in the frequency and intensity of extreme precipitation are projected across the entire region, and these increases are generally larger than the projected changes in average precipitation (Pryor et al., 2013).

The purpose of this work is to develop recommended hydrologic design standards that plan for future conditions based on the state-of-the-art climate change information. For example if the design standard calls for sizing stormwater controls based on a 10-year 24-hour event (3.77-inches) what is the rainfall depth of a 10-year 24-hour storm based on anticipated climate change scenarios? The specific objective is to (1) update the NOAA Atlas 14 precipitation frequency data, and (2) update the 90th percentile rainfall event to reflect the estimated future climate change information. This information may then be used to update the rainfall-based design criteria in the Grand Rapids Stormwater Technical Reference Manual.

(This page left intentionally blank.)

2 Methods

2.1 NOAA Atlas 14 IDF Curves

Intensity-Duration-Frequency (IDF) curves graphically summarize the relationship between precipitation intensity and the duration of precipitation events for a given frequency or recurrence interval. IDF curves provide important information for engineering design and planning purposes. In the U.S., official estimates of precipitation frequency for specific geographic locations are provided as IDF curves and tables in NOAA's Atlas 14 (Perica et al., 2013). The specific objective of this task is to update the NOAA Atlas 14 IDF curves for Grand Rapids, MI to reflect potential future changes in local climate. To satisfy this objective it is important to understand the way in which the Atlas 14 estimates were created. Specifically, frequency estimates in the Atlas are based on fitting a generalized extreme value (GEV) distribution to the time series of annual maximum precipitation (AMP) amounts at a station for seventeen durations ranging from 15 minutes to 60 days. The AMP series consists of one measurement per year, and does not account for the possibility of more than one event in a year exceeding a threshold of interest. The true probability of occurrence of events of a given intensity and duration should be derived from the partial duration series, which includes all events of a specified duration and above a pre-defined volume threshold. Frequency estimates for partial duration series were developed by NOAA from the series of AMPs using Langbein's conversion formula, which transforms a partial duration series-based average recurrence interval (ARI) to an annual exceedance probability (AEP):

$$AEP = 1 - \exp\left(-\frac{1}{ARI}\right) \quad (2\text{-}1)$$

Selected partial duration ARIs were first converted to AEPs using this formula, and frequency estimates were then calculated for the AEP using the GEV fit to annual maxima. This means that only the annual maximum series is needed for future climate conditions and not the complete or partial duration series.

NOAA fit the GEV for each station using the method of L-moments (Hosking and Wallis, 1997), incorporating regionalization across approximately the 10 nearest stations for higher order L-moments. NOAA intentionally does not release the fitted coefficients of the GEV distribution, although the annual maximum series are provided (see item 1.7 at http://www.nws.noaa.gov/oh/hdsc/FAQ.html).

It is important to note that the NOAA method is ultimately based only on annual maxima (the AMP series), and not analysis of continuous weather time series. This has important implications for the mathematical approach to updating the IDF curves, as described below.

2.2 Theoretical Basis for Updating IDF Curves

As noted above, the primary objective of this work is to evaluate potential changes to IDF curves in NOAA Atlas 14 under future climate, which requires understanding how the extreme value distribution fit to annual maximum precipitation series may change. Over the past decade researchers have proposed a variety of methods for updating IDF curves. These have generally been characterized by a high level of complexity and computational intensity, a lack of consensus, and concerns regarding whether non-stationarity is properly accounted for. Typically, the proposed methods have worked with complete future downscaled precipitation series, even though the Atlas 14 IDF curves depend only on the AMP series.

A simple, more direct, and computationally efficient approach to updating IDF curves was recently proposed by researchers at the University of Western Ontario (Srivastav et al., 2014a; Srivastav et al., 2014b). Their insight was that the essence of the problem was the need to update extreme value

distributions for future conditions, and that this could be done through a direct analysis of the distributions. The general concept of the approach of Srivastav et al. (2014a) is described as follows: "…quantile-mapping functions can be directly applied to establish the statistical relationship between the AMPs of GCM [Global Climate Model] and sub-daily observed data rather than using complete records. Further, the IDF is a distributional function; therefore it would be easy to derive the functional relationships between the distributions of the GCM AMPs and sub-daily observed data. One way of deriving such relationship is by using quantile-mapping functions. In this study we propose to use directly the annual maximum values for the baseline period and the projection period rather than using complete daily or sub-daily data."

Quantile mapping (QM) methods, otherwise known as cumulative distribution function (CDF) matching methods, have long been used as a method to correct for local biases in GCM output. The method first establishes a statistical relationship or transfer function between model outputs and historical observations, then applies the transfer function to future model projections (Panofsky and Brier, 1968) and has been successfully used as a downscaling method in various climate impact studies (e.g., Hayhoe et al., 2004).

Using the notation of Li et al. (2010), for a climate variable *x*, the method can be written as:

$$\hat{x}_{m-p.adjst.} = F_{o-c}^{-1}\left(F_{m-c}(x_{m-p})\right), \quad (2\text{-}2)$$

where *F* is the CDF of either the observations (o) or model (m) for observed current climate (c) or future projected climate (p). The bias correction for a future period is thus done by finding the corresponding percentile values for these future projection points in the CDF of the model for current observations, then locating the observed values for the same CDF values of the observations.

A potential weakness of this method is that it assumes that the climate distribution does not change much over time, and that, as the mean changes, the variance and skew do not change, which is likely not true (e.g., Milly et al., 2008). To address this, Li et al. (2010) proposed the equidistant quantile mapping (EQM) method, which incorporates additional information from the CDF of the model projection. The method assumes that the difference between the model and observed value during the current calibration period also applies to the future period; however, the difference between the CDFs for the future and historic periods is also taken into account. This is written as:

$$\hat{x}_{m-p.adjst.} = x_{m-p} + F_{o-c}^{-1}\left(F_{m-p}(x_{m-p})\right) - F_{m-c}^{-1}\left(F_{m-p}(x_{m-p})\right). \quad (2\text{-}3)$$

Appendix A in Srivastav et al. (2014b) provides MatLab code designed to update IDF curves in Canada. Their approach was found to be not directly applicable to our needs, for several reasons:

- Canada assumes that the AMP series follows a Gumbel, rather than a GEV distribution.
- Bias-corrected statistically downscaled climate model output is not widely available for Canada, therefore the Srivastav method must also incorporate a spatial downscaling step from the coarse scale of GCMs, whereas we can use output that is already spatially downscaled to a fine resolution grid for the US.
- The method of Srivastav et al. claims to implement EQM, but largely consists of a multi-step QM procedure, without the additional EQM corrections.

Given these considerations, we began with the conceptual code of Srivastav et al. (2014b), but re-derived it as an EQM procedure for use in the U.S. as described in the next section.

2.3 ATLAS 14 IDF CURVES UPDATE APPROACH USING GENERALIZED EXTREME VALUE DISTRIBUTION

A combination of EQM and QM approaches were used to update IDF curves for Grand Rapids conditional on output of GCMs for future climate conditions. Calculations were implemented in Python code. Two mapping steps are needed to update IDF curves. We begin with model output that has already been subject to spatial bias correction and downscaling to a 4x4 km spatial scale and daily time step (see Section 3.2). The first step consists of additional spatial downscaling from the 4x4 km grid to the specific location of the Grand Rapids International Airport weather station used by Atlas 14 along with bias correction for the AMP series (as distinct from the general bias correction of the complete precipitation series) using the EQM method. The second step consists of temporal downscaling to sub-daily durations using the QM method (EQM is not needed for this step because it does not involve bias correction).

For the first step, the historical data are the AMP series used by Atlas 14 and extracted from the records at the Grand Rapids International Airport station (X_{max}^{STN}). Model data include the predicted AMP series for the same historical period (X_{max}^{GCM}) and for the future period of interest ($X_{max}^{GCM_{FUT}}$). A GEV distribution is fit to each of these series, using the L-moments method, consistent with Atlas 14:

$$\boldsymbol{Prob(STN) = f\left(\theta^{STN}, X_{max}^{STN}\right)} \quad (2\text{-}4)$$

$$\boldsymbol{Prob(GCM) = f\left(\theta^{GCM}, X_{max}^{GCM}\right)} \quad (2\text{-}5)$$

$$\boldsymbol{Prob(GCM_{FUT}) = f\left(\theta^{GCM_{FUT}}, X_{max}^{GCM_{FUT}}\right)} \quad (2\text{-}6)$$

where $f(\ )$ is the probability density function, and θ represents the parameter of the fitted distribution.

To apply the EQM method, quantiles of modeled future daily extreme data are matched to the distribution for historical AMPs. For a given percentile, we assume that the difference between the model and observed value also applies to the future period and calculate the two EQM factors for Equation (2-3).

$$\boldsymbol{Y_{max}^{adj1} = F_{o-c}^{-1}\left(F_{m-p}\left(x_{m-p}\right)\right) = invCDF((CDF\left(X_{max}^{GCM_{FUT}}|\theta^{GCM_{FUT}}\right))|\theta^{STN\_daily}),} \quad (2\text{-}7)$$

where the vertical bar "|" indicates conditional dependence, i.e., $CDF\left(X_{max}^{GCM_{FUT}}|\theta^{GCM_{FUT}}\right)$ indicates the cumulative distribution function of the future GCM AMP series using the parameter set calculated for that future series. To account for the difference between the *CDFs* for the model outputs of future and current periods, the second adjustment factor was calculated.

$$\boldsymbol{Y_{max}^{adj2} = F_{m-c}^{-1}\left(F_{m-p}\left(x_{m-p}\right)\right) = invCDF((CDF\left(X_{max}^{GCM_{FUT}}|\theta^{GCM_{FUT}}\right))|\theta^{GCM})} \quad (2\text{-}8)$$

The projected AMP series are then calculated using the approach of Equation (2-3) as implemented in Equation (2-9):

$$\boldsymbol{Y_{max}^{STN\_FUT\_daily} = X_{max}^{GCM\_FUT} + Y_{max}^{adj1} - Y_{max}^{adj2}} \quad (2\text{-}9)$$

The second step is temporal downscaling to convert future daily extremes into sub-daily extremes. The QM method was used for this purpose. We first find the corresponding percentile values for these future projection points in the CDF of the model for the historical period, then locate the observed values for the same CDF values of the sub-daily observations. For rainfall duration *i*:

$$Y_{max,i}^{STN\_FUT\_subdaily} = invCDF((CDF\left(Y_{max}^{STN_{FUT_{daily}}}|\theta^{STN_{daily}}\right))|\theta_i^{STN\_subdaily}) \quad (2\text{-}10)$$

As noted in Atlas 14 (Perica et al., 2013) estimates for shorter durations can be noisy due to limited data availability and are improved by smoothing. The projected future sub-daily extreme values were thus smoothed by fitting them to the daily extreme projection of the station by linear regression:

$$Y_{max,i}^{STN\_FUT\_subdaily} = a_1 * Y_{max}^{STN\_FUT\_daily} + b_1 \quad (2\text{-}11)$$

After $Y_{max,i}^{STN\_FUT\_subdaily}$ were calculated, GEV distributions were used to fit the extremes projections. Then rainfall amounts at certain probabilities were extracted to create the rainfall series with different recurrence intervals:

$$Y_{max,i,p}^{STN\_FUT\_subdaily} = invCDF(1-p, (CDF\left(Y_{max,i}^{STN\_FUT\_subdaily}\right))) \quad (2\text{-}12)$$

where *p* is the AEP corresponding to the desired recurrence interval (Equation 2-1).

The changing ratio and rainfall extremes between current and future can then be derived by comparing the derived historical rainfall extremes at different reoccurrence intervals based on observation data $X_{max,i,p}^{STN}$ with the spatial and temporal downscaled GCM rainfall extremes data $Y_{max,i,p}^{STN\_FUT\_subdaily}$.

$$\mathbf{R}_{i,p}^{j} = \frac{Y_{max,i,p}^{STN\_FUT\_subdaily,j}}{X_{max,i,p}^{STN}} \quad (2\text{-}13)$$

where *j* represents the underlying GCM. The IDF curves are then updated by multiplying the rainfall maxima from Atlas 14 by the changing ratios for the different GCMs.

For durations less than one hour, Atlas 14 (Perica et al., 2013) relates 15 and 30-minute durations to the 60-minute duration using local scaling factors:

$$\mathbf{S} = \frac{X_k^{Atlas\_14}}{X_{60-mintue}^{Atlas\_14}} \quad \text{, k=15-minute or 30 minute} \quad (2\text{-}14)$$

Fixed scaling factors are used for deriving 10-minute and 5-minute annual maxima. The ratio of the10-minute annual maximum to the 15-minute annual maximum is assumed to be 0.82 and the ratio for the 5-minute annual maxima is 0.57.

2.4 90TH PERCENTILE RAINFALL EVENT UPDATE APPROACH USING GENERALIZED PARETO DISTRIBUTION

Grand Rapids also uses the 90th percentile rainfall event for planning and design purposes. The current estimate of the volume of this event is 0.99 in., derived from analysis of daily precipitation records from Grand Rapids International Airport (Station ID 20 3333) for the period from Jan 1949 through April 2013 and excluding non-runoff generating events (assumed to be <= 0.10 inches). It is important to note that the method is based on daily rainfall, and not on specifically defined events that may overlap days.

The 90th percentile event occurs much more frequently than the AMP (on average, 10% of the events per year will exceed this event), thus a GEV analysis based only on AMP is not appropriate for this measure; however, an EQM approach similar to that used for IDF curves can be applied for future updates. The distribution of the 90th percentile event can be described by a Peaks-over-Threshold (POT) approach, which characterizes the frequency of events greater than a specified magnitude (Serinaldi and Kilsby, 2014). As the value of the threshold (u) increases, the distribution of the POT (prob $Y := (X\text{-}u)|X > u$) converges to a generalized Pareto distribution (GPD; Pickands, 1985; Balkema and de Haan, 1974):

$$\boldsymbol{H(y) = 1 - \left(1 + \xi \frac{y}{\tilde{\sigma}}\right)^{-1/\xi}}, \quad \text{(2-15)}$$

in which $\{y: y > 0$ and $1 + \xi \frac{y}{\tilde{\sigma}} > 0\}$ and $\tilde{\sigma} = \sigma + \xi(u - \mu)$, μ is the location parameter, $\sigma > 0$ is the scale parameter, and ξ is the shape parameter.

A few assumptions were necessary to apply the GPD/POT method.

1. The exceedances are independent and identically distributed.
2. The threshold is sufficiently large that the tails asymptote to the limit distribution.

We limited our sample pool only to larger rainfall events, so temporal correlation (non-independence) is not a major concern. The selection of threshold is then crucial for the application of POT method. We selected the threshold to meet condition (2) based on the stability of GPD parameters as recommended by Serinaldi and Kilsby (2014). At sufficiently large threshold, the shape and modified scale parameters of GPD distribution are independent of the threshold. Different thresholds were applied to the rainfall records, and the GPD was fit at each threshold level. The derived shape and modified scale parameters with different thresholds values are shown in Figure 1 and Figure 2. The parameters are relatively stable if the threshold is larger than 0.2 inch, so 0.2 inch was used as the threshold for POT method in this project.

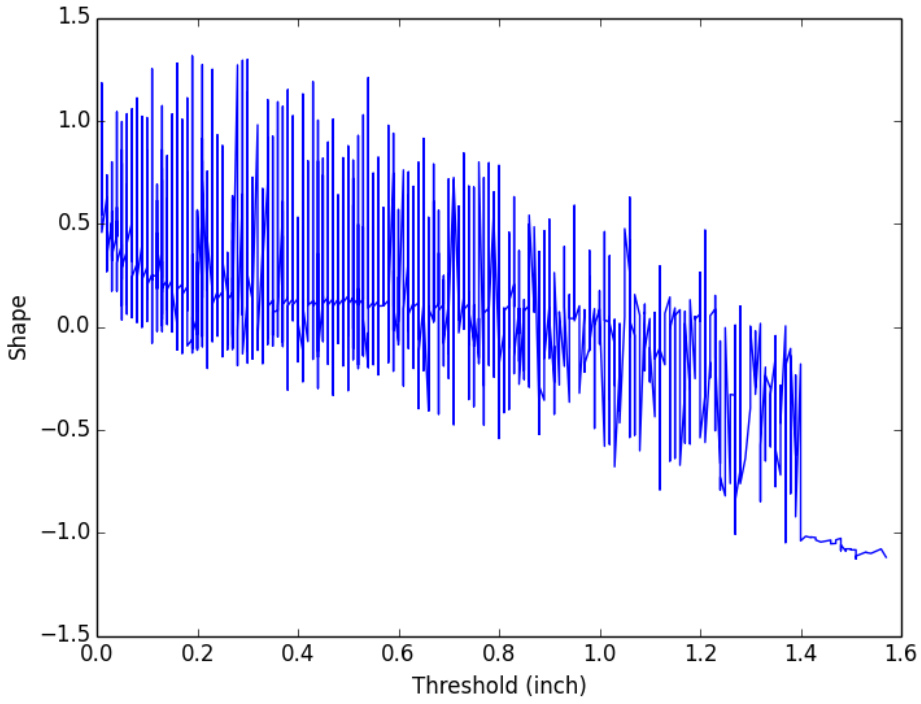

Figure 1. GPD Shape Parameters Derived with Varying Thresholds

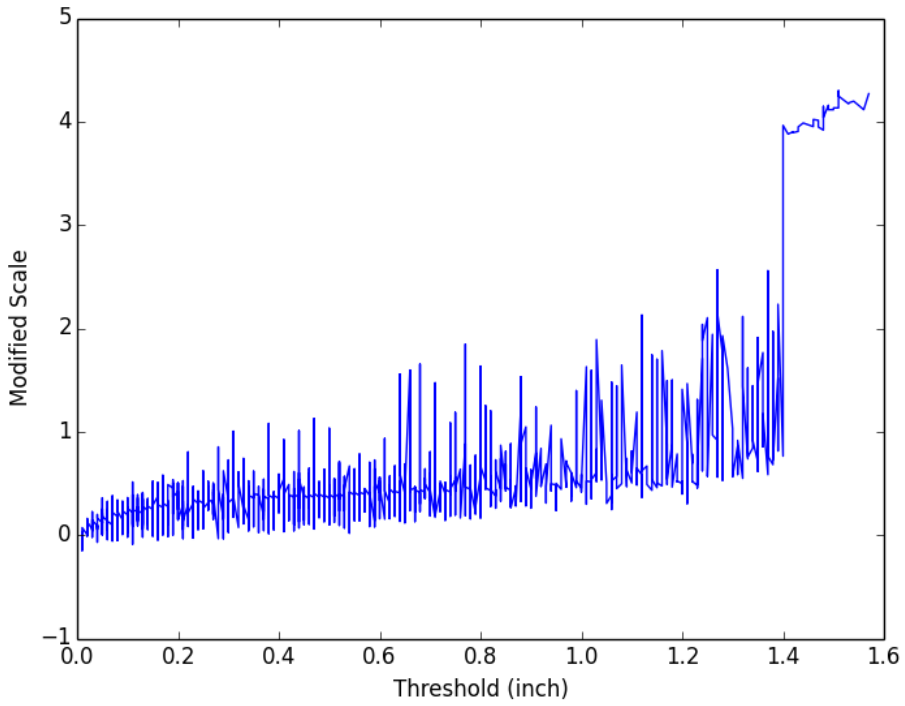

Figure 2. GPD Scale Parameters Derived with Varying Thresholds

Rainfall records above 0.2 inch were extracted from the daily rainfall dataset (both observed and model simulated) and were used to fit the GPD. A conditional distribution can be written for rainfall events (x > *u*) above *u* = 0.2 inches as:

$$\boldsymbol{Prob}(\boldsymbol{X} > \boldsymbol{x} | \boldsymbol{X} > \boldsymbol{u}) = \mathbf{1} - \boldsymbol{GPD}(\boldsymbol{x} - \boldsymbol{u};\ \boldsymbol{\sigma}, \boldsymbol{\xi}). \quad (2\text{-}16)$$

After the GPD distributions were fit to observed and modelled daily rainfall data, equations (2-7), (2-8), and (2-9) for implementing EQM can be applied, substituting the GPD for the GEV distribution, to complete the spatial downscaling and bias correction for the Grand Rapids International Airport station. The downscaled POT records also follows GPD and were fit with GPD to get the conditional distribution. Equation (2-17) was used to estimate an unconditional distribution and return value:

$$\boldsymbol{Prob}(\boldsymbol{X} > \boldsymbol{x}) = \boldsymbol{Prob}(\boldsymbol{x} > \boldsymbol{u}) * (\mathbf{1} - \boldsymbol{GPD}(\boldsymbol{x} - \boldsymbol{u}; \boldsymbol{\sigma}, \boldsymbol{\xi})) \quad (2\text{-}17)$$

where $Prob(x > u)$ could be estimated using the ratio between length of rainfall records above threshold and the full rainfall records. After the probabilities and amounts of rainfall from unconditional distribution were derived using Equation (2-17). The 90th percentile rainfall amount estimated by each GCM was calculated using linear interpolation:

$$\boldsymbol{X_{90}} = \frac{\boldsymbol{Prob_{90}} - \boldsymbol{Prob_{90-}}}{\boldsymbol{Prob_{90+}} - \boldsymbol{Prob_{90-}}} * (\boldsymbol{X_{90+}} - \boldsymbol{X_{90-}}), \quad (2\text{-}18)$$

where X_{90+} and X_{90-} are the observations closest above and below the 90th percentile in the rainfall series.

3 Future Climate Scenarios

3.1 SELECTION OF FUTURE CLIMATE SCENARIOS

In 2013, a Climate Resiliency Report for Grand Rapids was prepared by the West Michigan Environmental Action Council (WMEAC). This report used the Model for the Assessment of Greenhouse-gas Induced Climate Change and Regional Scenario Generator (MAGICC/SCENGEN; Wigley, 2008) to forecast potential changes in annual and seasonal temperature and precipitation in Grand Rapids through 2042. The MAGICC portion "is an upwelling-diffusion, energy-balance model that produces global- and hemispheric-mean temperature output together with results for oceanic thermal expansion." The SCENGEN portion then converts the global output to a more local result using a pattern scaling method that relies on the data base of output from the suite of global climate models (GCMs) produced for the Intergovernmental Panel on Climate Change (IPCC)'s 4th Reassessment Report (2007) as part of the Coupled Model Intercomparison Project round 3 (CMIP3). These results are presented at a rather coarse spatial scale of 2.5°x2.5° (about 175 x 175 miles). Temporally, only seasonal results are provided, and the Resiliency Report notes "MAGICC/SCENGEN has a significant limitation in that it deals in seasonal averages and is not capable of forecasting extreme weather trends." Both the spatial and temporal scale of this product make it insufficient for evaluating changes in IDF of precipitation.

Since production of the Resiliency Report, the IPCC (2013) has released the 5th Reassessment Report, incorporating results from a new round of GCM runs (CMIP5). CMIP5 incorporates a number of refinements to the GCMs. It also uses a different set of greenhouse gas concentration scenarios than the emissions-based scenarios that were used in CMIP3. These greenhouse gas scenarios are now referred to as Representative Concentration Pathways (RCPs) and are based on a future target radiative forcing rather than inferring the radiative forcing (e.g., RCP 4.5 represents radiative forcing of 4.5 W/m^2 in year 2100) from uncertain projections of future population growth, energy use patterns, and associated greenhouse gas emissions.

We recommend using the newest CMIP5 model results for the purpose of updating IDF curves. In addition to incorporating the latest model updates the CMIP5 results are now available in a variety of online repositories that enable rapid screening of the range of potential future outcomes predicted by the suite of GCMs. There is also a desire, however, to maintain consistency with the Resiliency Report. The analysis in the Resiliency Report used the emissions scenario known as A1B, which was a middle-of-the-road emissions scenario incorporating "balanced emphasis on all energy sources." There is not an exact match to this scenario in CMIP5; however, the projected greenhouse gas trajectory under A1B is bounded above and below by RCP 8.5 and RCP 4.5.

RCP 8.5 includes higher greenhouse gas concentrations, and thus greater radiative forcing and higher global atmospheric temperatures than RCP 4.5; however, the difference among individual GCMs is generally greater than the difference between RCP 4.5 and RCP 8.5 projections through at least the middle of the 21st century. Further, the greatest impacts on precipitation do not necessarily line up with increases in temperature, and for various GCMs the increase in rainfall volume is greater with RCP 4.5 than for RCP 8.5 for the 2050-2070 period (although physics suggest maximum intensity is more likely to occur with the higher temperature scenario). We therefore screened across the output of the 30-some GCMs applied to both RCP 4.5 and RCP 8.5 to identify a smaller set for detailed analysis at Grand Rapids.

Future climate projections are uncertain and are best used to describe a probability envelope of potential future conditions (an "ensemble of opportunity"; Mote et al., 2011) to which adaptation may be needed. Accordingly, we screened for climate scenarios that approximate smaller, median, and larger range of potential changes in precipitation intensity. Specifically, we selected sets of two scenarios (one from

RCP 4.5 and one from RCP 8.5) that appear to be near the 10th, 50th, and 90th percentiles of the distribution among GCMs of annual extreme precipitation in the Grand Rapids area. Ranking was evaluated based on both the largest daily extreme and average daily extreme across the 30-year time window. We selected the 10th and 90th percentiles, rather than the most extreme models, as it is well recognized that some individual GCMs may provide unrealistic results for a given area. It is therefore standard practice to ignore the most extreme outliers and use a model at approximately the 90th percentile of the complete set of models as a reasonable upper bound. Use of such an upper percentile is generally considered appropriate for engineering/hydrologic design planning purposes; however, the full range may also be of interest.

For future time periods we examined the mid-21st century and the end of the century. CMIP5 model projections run through 2100; however, they also incorporate decadal cyclical drivers of climate variability, so change evaluations can't be based on a single year. Therefore, we examine 30-year time slices centered at 2050 and 2085 to represent mid- and late-century conditions.

Initial screening across 30 GCMs and 2 RCPs must be done in an efficient manner to accommodate the project budget. Our primary interest is in maximum precipitation rates, not total monthly or annual precipitation volume. Therefore, the initial screening was based on non-downscaled GCM results for maximum 1-day precipitation (by year and geographic location) extracted by the Expert Team on Climate Change Detection and Indices (Sillmann et al., 2013a, 2013b) and served as CLIMDEX by Environment Canada (http://www.cccma.ec.gc.ca/data/climdex/climdex.shtml). The anomalies (difference from present) in these extremes show a wide spread among GCMs (Figure 1

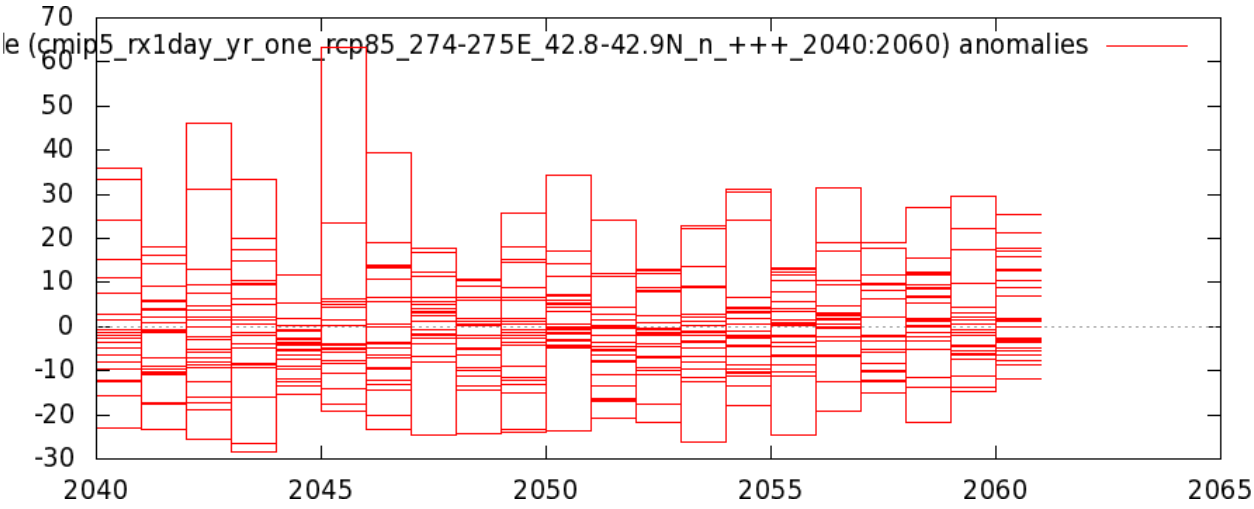

Figure 3. Model Ensemble Distribution of Annual 1-day Maximum Precipitation for Grand Rapids, MI Area

Note: Results extracted from CLIMDEX by Climate Explorer (http://climexp.knmi.nl).

We have not used measures of GCM skill or quality of performance in replicating past climate for the Midwest as primary criterion for model selection. In addition to the fact that performance on past climate is not necessarily a good predictor of future performance, Mote et al. (2011) have demonstrated that attempting to select GCMs based on performance does not appear to reduce uncertainty in projections. We did, however, introduce some additional criteria for selecting among the set of models near each of the percentile targets. Specifically, we favored, where available GCMs that use a finer spatial resolution or are among those with a better apparent fit in predicting summer precipitation (Toreti et al., 2013), both of which are likely to be associated with better prediction of summer convective storms. We also favored GCMs demonstrated to have low global Bias ($0.9 < B < 1.1$) and a high volumetric hit index ($VHI > 0.7$) for mean monthly precipitation (Mehran et al., 2014). The selected GCMs are shown in Table 1.

Table 1. GCMs Selected for Detailed Analysis

Percentile	RCP 8.5 Models	RCP 4.5 Models
90%	RCP8.5 MIROC5 (a)	RCP4.5 IPSL-CM5B-LR
50%	RCP8.5 CNRM-CM5 (a, b)	RCP4.5 CNRM-CM5 (a, b)
10%	RCP8.5 bcc-csm1-1 (b)	RCP4.5 bcc-csm1-1 (b)

Notes: a. High-resolution (Toreti et al., 2013); b. Low bias, high volumetric hit index (Mehran et al., 2014)

It should be noted that rankings on final analysis of the magnitude of storms of a given intensity and duration from downscaled GCM output may not follow the same order as shown in the CLIMDEX screening of non-downscaled GCMs. This occurs because the GCM output is subject to local bias correction during the downscaling process. As a result of this, a GCM that has lower peak rainfall intensity in the raw output could actually yield higher peak intensity in downscaled output if the bias correction factor is larger than that for other competing models. Nonetheless, sampling across a range of GCM behavior is useful to help ensure an inclusive data set. We suggest that final future IDF curves for application should be selected from the largest responses observed in the six model sample set described above, regardless of the ranking of the un-downscaled GCM, to provide reasonably protective design standards.

3.2 SPATIALLY DOWNSCALED CLIMATE DATA

GCM's generate output at a large spatial scale (typically about 1°x1° or coarser) that does not take into account details of local geography and topography. To be useful at the local scale it is necessary to undertake spatial downscaling. Downscaling can be done either through the use of a small-scale regional climate model (RCM) or through statistical methods. RCMs are difficult and expensive to run, so only a limited number of GCMs have been downscaled in this way. In contrast, there are many different varieties of statistically downscaled products now available. Most of these work with the general design of using spatial statistical corrections of GCM monthly output to local spatial scales with bias correction based on analysis of GCM ability to replicate historical climatology, followed by temporal downscaling to a daily time step. A recent recommendation from the U.S. Fish and Wildlife Service (Patte, 2014) is to use the Multivariate Adaptive Constructed Analogs (MACA) statistically downscaled data (to a 4 km x 4 km scale) created by the University of Idaho. The MACA method (Abatzoglou and Brown, 2012) has two advantages that make it slightly preferable to other downscaling methods: (1) it provides simultaneous downscaling of precipitation, temperature, humidity, wind, and radiation (rather than just precipitation and temperature), helping to ensure physical consistency in the outputs, and (2) the method uses a historical library of observations to construct the downscaling in the constructed analogs approach such that future climate projections are distributed from the monthly to the daily scale in comparison to months that exhibit similar characteristics in the historical record. We therefore retrieved downscaled GCM output for the location of Grand Rapids International Airport (the observing station from which Atlas 14 results for the area are calculated) from the MACA website (http://maca.northwestknowledge.net/). From these results we extracted the AMP series and POT series for calculation of updated IDF curves and revised 90th percentile event volumes.

(This page left intentionally blank>0

4 Results

The methods described in Sections 2.3 and 2.4 were applied to the MACA output of spatially downscaled climate data for the GCMs identified in Section 3.1 to estimate the potential range of IDF curves and 90th percentile events for the time periods around 2050 and 2085. The year 2050 was chosen as representative of mid-century conditions based on climate models from 2035 to 2064. Climate model archives run through 2100, the last 30 years (centered at 2085) was selected as representative of trends toward the end of the century. IDF curves were calculated for 2, 5, 10, 25, 50, 100, 200, 500, and 1000-year events at variety of durations ranging up to 24 hours. Results are presented in graphical and tabular format in Sections 4.1 through 4.4.

Note that the two CNRCM-CM5 GCM scenarios, although characterized as "middle of the road" in initial screening for future event intensity in Section 3.1, provide the highest predictions of intensity for specified durations across most recurrence frequencies under projected 2050 conditions. This occurs because the spatially downscaled and bias corrected output of CNRCM-CM5 predicts larger average AMPs and a relatively larger increase in AMPs between historic and 2050 conditions than does the output for other models such as MIROC-5.

4.1 IDF CURVES FOR 2050

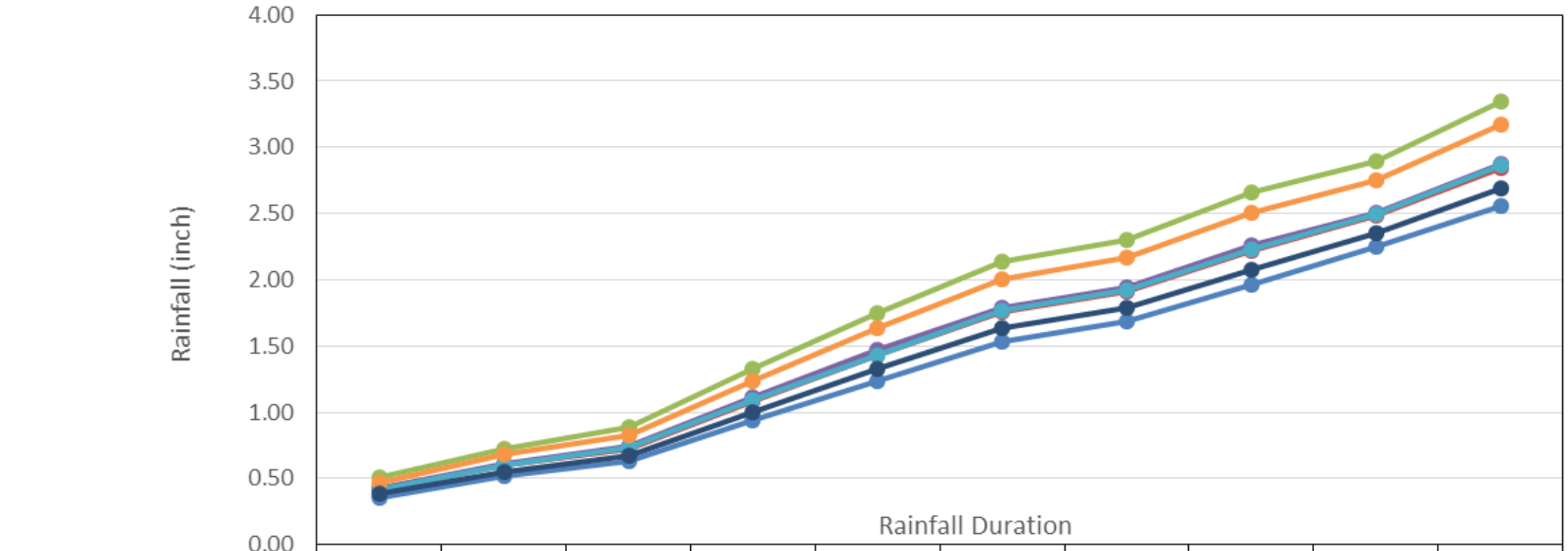

	5-min	10-min	15-min	30-min	1-hr	2-hr	3-hr	6-hr	12-hr	24-hr
NOAA Atlas 14	0.35	0.52	0.63	0.94	1.24	1.53	1.69	1.96	2.25	2.56
MIROC5, RCP8.5	0.42	0.60	0.73	1.09	1.43	1.76	1.91	2.22	2.48	2.84
CNRM-CM5, RCP 8.5	0.51	0.73	0.89	1.32	1.75	2.13	2.30	2.66	2.90	3.34
BCC-CSM-1-1, RCP 8.5	0.43	0.61	0.75	1.11	1.47	1.79	1.94	2.26	2.51	2.88
IPSL-CM5B-LR, RCP 4.5	0.42	0.60	0.73	1.09	1.43	1.77	1.93	2.23	2.50	2.86
CNRM-CM5, RCP 4.5	0.47	0.68	0.83	1.24	1.63	2.00	2.17	2.50	2.76	3.17
BCC-CSM-1-1, RCP 4.5	0.38	0.55	0.67	1.00	1.33	1.63	1.79	2.08	2.35	2.69

Figure 4. Updated 2050 IDF Curves for 2-year Recurrence Precipitation at Grand Rapids, MI

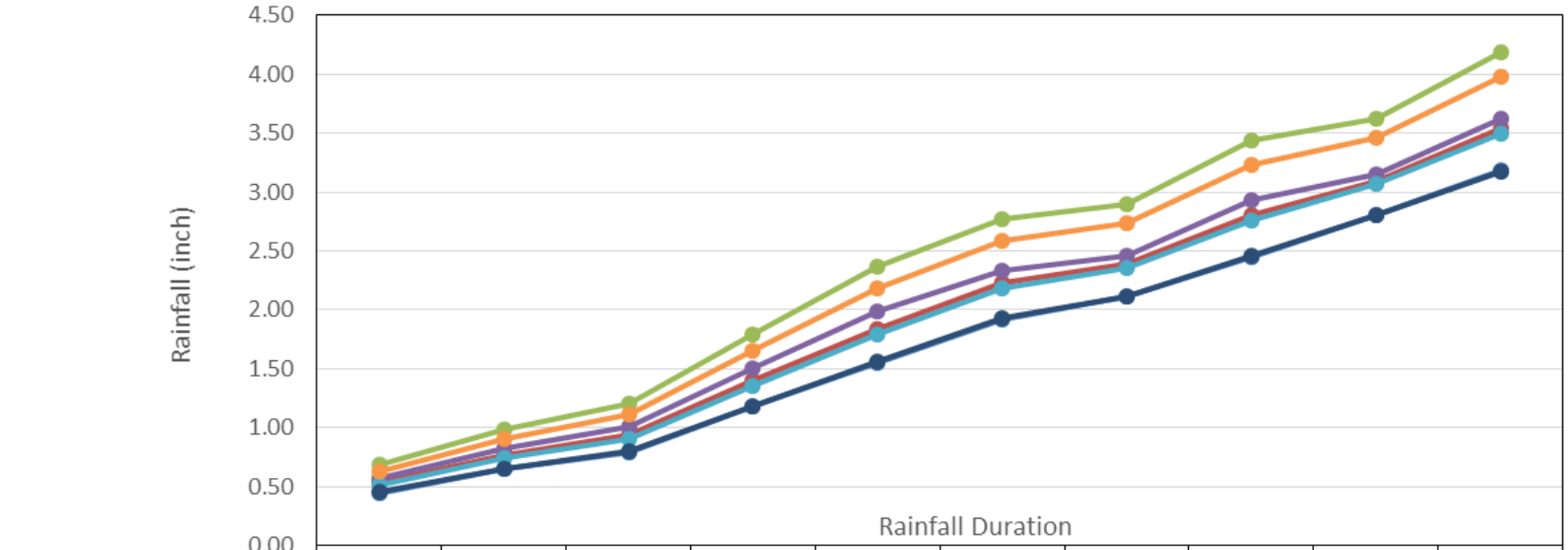

	5-min	10-min	15-min	30-min	1-hr	2-hr	3-hr	6-hr	12-hr	24-hr
NOAA Atlas 14	0.44	0.65	0.79	1.18	1.55	1.92	2.11	2.45	2.81	3.18
MIROC5, RCP8.5	0.53	0.77	0.94	1.40	1.84	2.23	2.39	2.81	3.10	3.54
CNRM-CM5, RCP 8.5	0.68	0.98	1.20	1.79	2.36	2.77	2.89	3.44	3.63	4.19
BCC-CSM-1-1, RCP 8.5	0.57	0.83	1.01	1.51	1.99	2.34	2.46	2.93	3.15	3.62
IPSL-CM5B-LR, RCP 4.5	0.52	0.74	0.91	1.35	1.79	2.18	2.36	2.75	3.07	3.50
CNRM-CM5, RCP 4.5	0.63	0.91	1.11	1.65	2.18	2.59	2.73	3.24	3.46	3.99
BCC-CSM-1-1, RCP 4.5	0.45	0.65	0.79	1.19	1.56	1.93	2.11	2.46	2.80	3.18

Figure 5. Updated 2050 IDF Curves for 5-year Recurrence Precipitation at Grand Rapids, MI

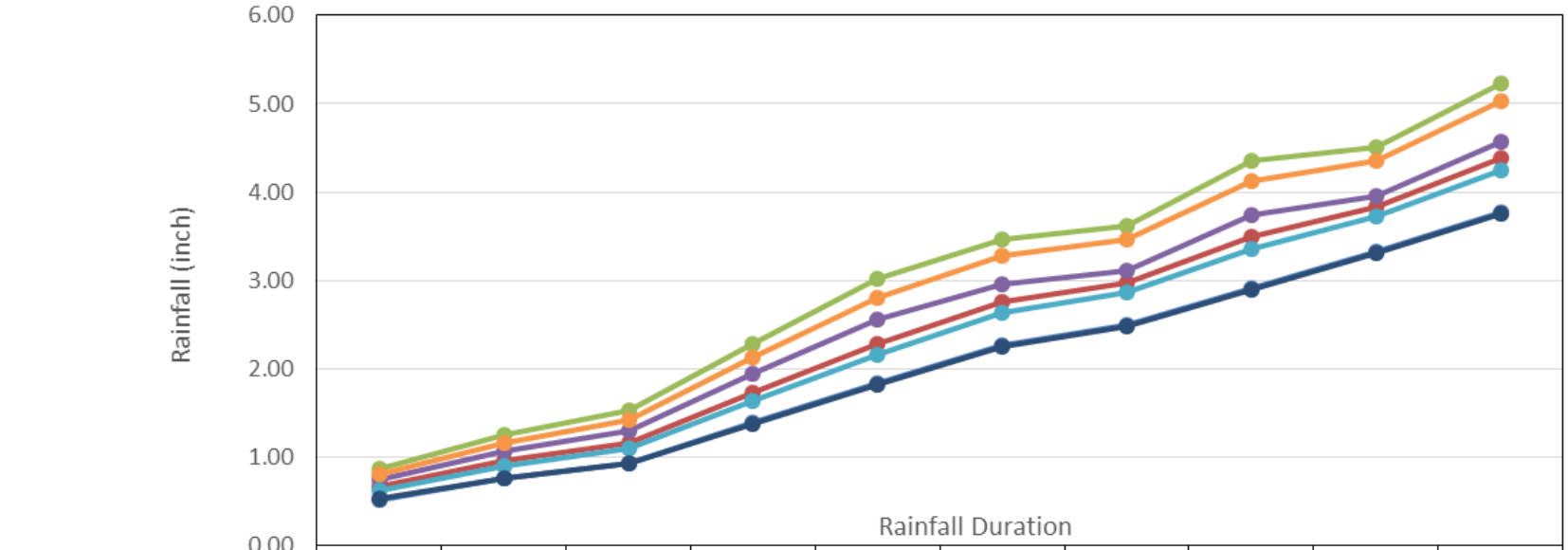

	5-min	10-min	15-min	30-min	1-hr	2-hr	3-hr	6-hr	12-hr	24-hr
NOAA Atlas 14	0.52	0.76	0.93	1.39	1.83	2.26	2.50	2.91	3.33	3.77
MIROC5, RCP8.5	0.66	0.95	1.16	1.73	2.29	2.75	2.97	3.50	3.84	4.39
CNRM-CM5, RCP 8.5	0.87	1.25	1.53	2.28	3.01	3.47	3.62	4.35	4.51	5.23
BCC-CSM-1-1, RCP 8.5	0.74	1.07	1.30	1.94	2.56	2.96	3.12	3.74	3.95	4.56
IPSL-CM5B-LR, RCP 4.5	0.62	0.90	1.09	1.63	2.15	2.63	2.86	3.35	3.73	4.25
CNRM-CM5, RCP 4.5	0.81	1.16	1.42	2.12	2.80	3.28	3.46	4.13	4.35	5.03
BCC-CSM-1-1, RCP 4.5	0.53	0.76	0.92	1.37	1.81	2.24	2.49	2.89	3.32	3.75

Figure 6. Updated 2050 IDF Curves for 10-year Recurrence Precipitation at Grand Rapids, MI

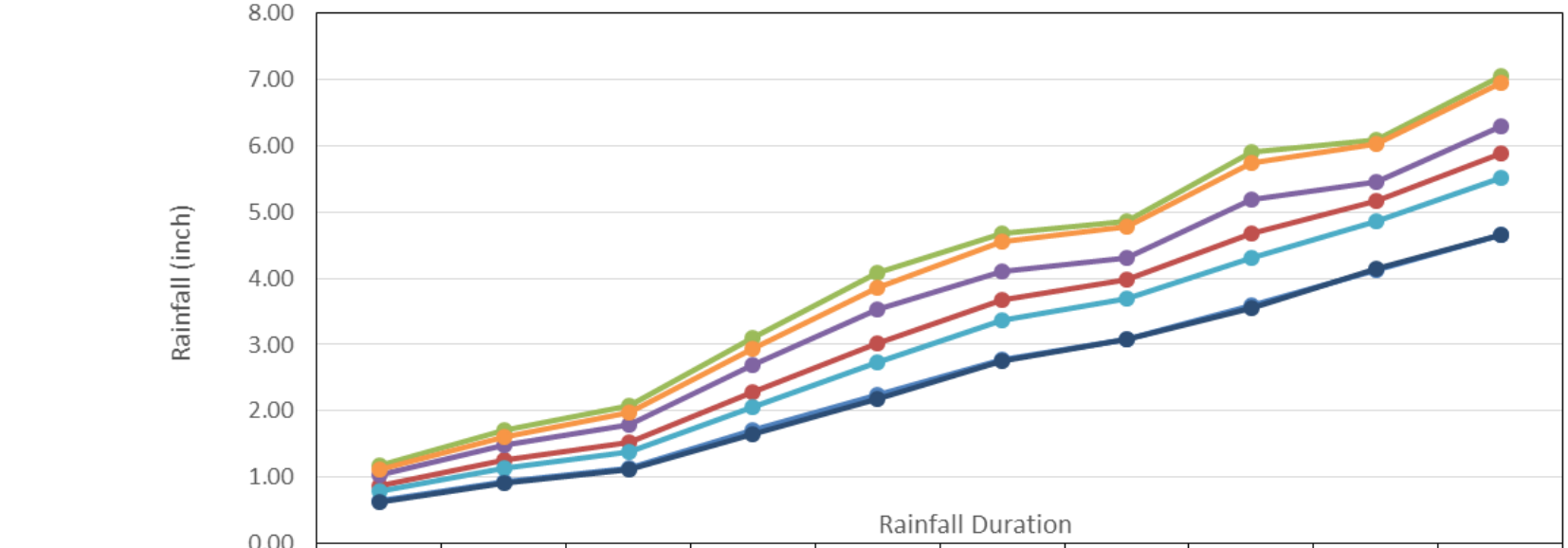

	5-min	10-min	15-min	30-min	1-hr	2-hr	3-hr	6-hr	12-hr	24-hr
NOAA Atlas 14	0.64	0.93	1.14	1.70	2.24	2.78	3.08	3.60	4.13	4.66
MIROC5, RCP8.5	0.87	1.26	1.53	2.29	3.02	3.67	3.98	4.68	5.16	5.89
CNRM-CM5, RCP 8.5	1.18	1.70	2.07	3.09	4.08	4.69	4.87	5.91	6.09	7.06
BCC-CSM-1-1, RCP 8.5	1.03	1.48	1.80	2.68	3.54	4.10	4.30	5.20	5.45	6.29
IPSL-CM5B-LR, RCP 4.5	0.79	1.14	1.38	2.07	2.72	3.37	3.70	4.32	4.86	5.51
CNRM-CM5, RCP 4.5	1.12	1.61	1.96	2.93	3.87	4.55	4.79	5.74	6.03	6.96
BCC-CSM-1-1, RCP 4.5	0.63	0.91	1.11	1.65	2.18	2.74	3.08	3.56	4.16	4.67

Figure 7. Updated 2050 IDF Curves for 25-year Recurrence Precipitation at Grand Rapids, MI

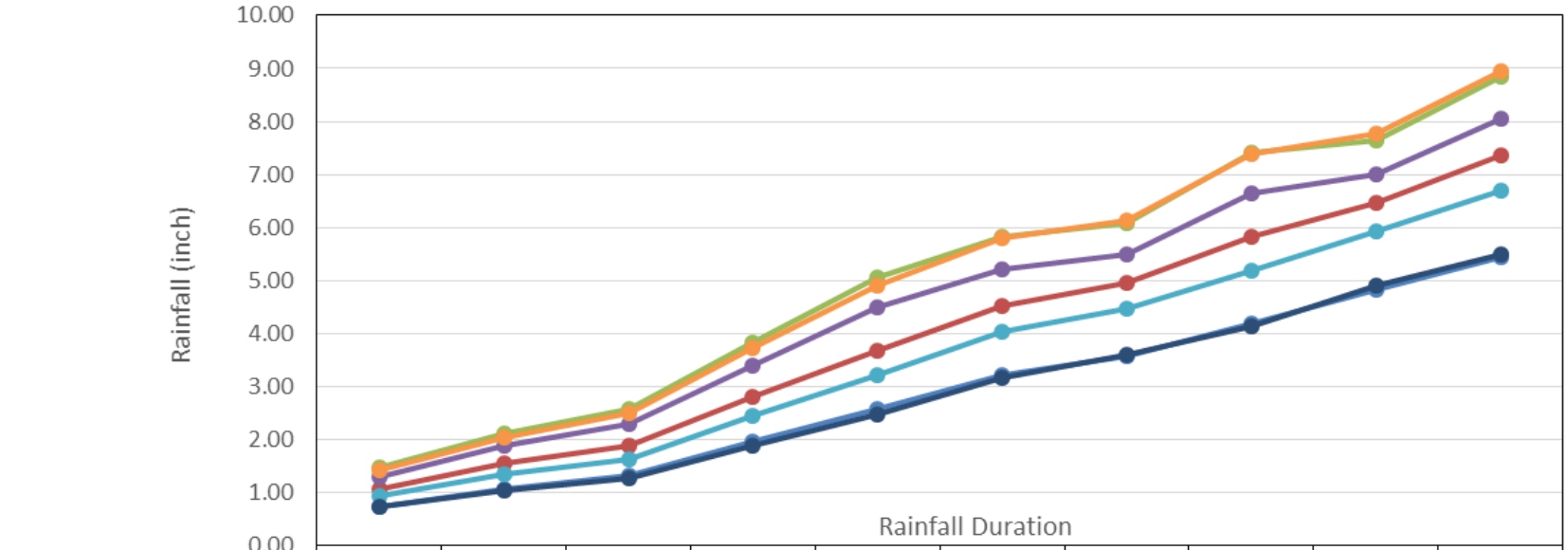

	5-min	10-min	15-min	30-min	1-hr	2-hr	3-hr	6-hr	12-hr	24-hr
NOAA Atlas 14	0.73	1.07	1.31	1.95	2.58	3.21	3.57	4.19	4.82	5.43
MIROC5, RCP8.5	1.07	1.53	1.87	2.79	3.68	4.52	4.95	5.81	6.47	7.35
CNRM-CM5, RCP 8.5	1.47	2.11	2.57	3.84	5.06	5.83	6.09	7.41	7.65	8.86
BCC-CSM-1-1, RCP 8.5	1.30	1.87	2.28	3.40	4.49	5.22	5.50	6.66	6.99	8.05
IPSL-CM5B-LR, RCP 4.5	0.93	1.34	1.63	2.44	3.22	4.02	4.46	5.20	5.92	6.68
CNRM-CM5, RCP 4.5	1.42	2.05	2.49	3.72	4.91	5.80	6.14	7.38	7.77	8.95
BCC-CSM-1-1, RCP 4.5	0.72	1.03	1.26	1.88	2.48	3.16	3.59	4.14	4.91	5.48

Figure 8. Updated 2050 IDF Curves for 50-year Recurrence Precipitation at Grand Rapids, MI

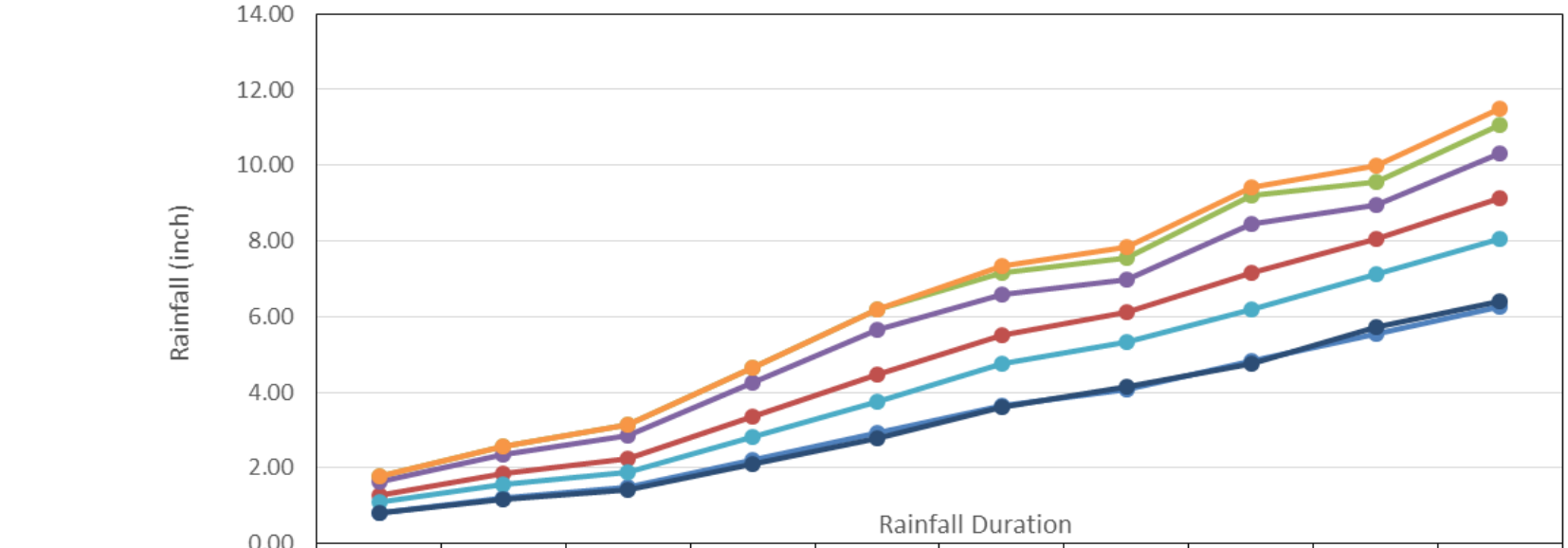

	5-min	10-min	15-min	30-min	1-hr	2-hr	3-hr	6-hr	12-hr	24-hr
NOAA Atlas 14	0.83	1.22	1.49	2.21	2.94	3.66	4.09	4.82	5.56	6.27
MIROC5, RCP8.5	1.29	1.85	2.26	3.35	4.45	5.52	6.11	7.16	8.04	9.13
CNRM-CM5, RCP 8.5	1.79	2.58	3.15	4.67	6.21	7.17	7.54	9.20	9.55	11.06
BCC-CSM-1-1, RCP 8.5	1.63	2.34	2.86	4.24	5.64	6.58	6.99	8.46	8.93	10.30
IPSL-CM5B-LR, RCP 4.5	1.09	1.56	1.90	2.82	3.76	4.74	5.33	6.19	7.14	8.05
CNRM-CM5, RCP 4.5	1.79	2.57	3.13	4.65	6.18	7.34	7.84	9.42	9.97	11.50
BCC-CSM-1-1, RCP 4.5	0.80	1.16	1.41	2.09	2.78	3.60	4.14	4.75	5.73	6.39

Figure 9. Updated 2050 IDF Curves for 100-year Recurrence Precipitation at Grand Rapids, MI

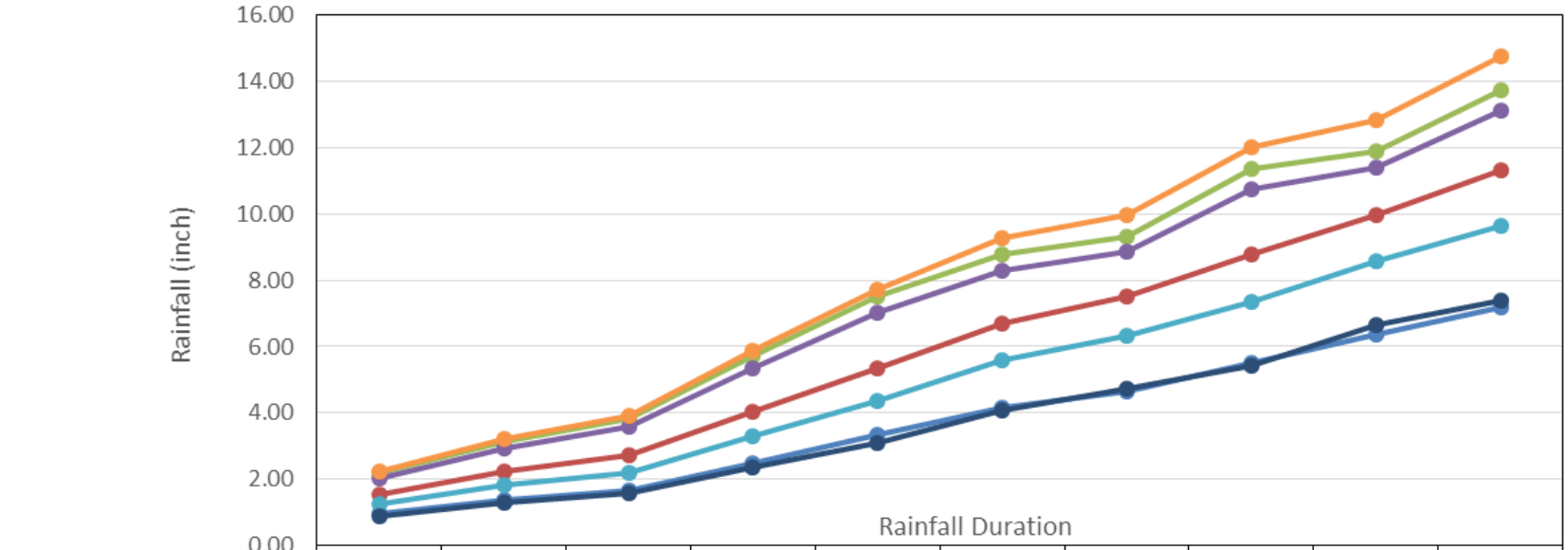

	5-min	10-min	15-min	30-min	1-hr	2-hr	3-hr	6-hr	12-hr	24-hr
NOAA Atlas 14	0.94	1.37	1.67	2.49	3.32	4.15	4.65	5.52	6.38	7.19
MIROC5, RCP8.5	1.55	2.22	2.71	4.05	5.34	6.71	7.50	8.79	9.99	11.31
CNRM-CM5, RCP 8.5	2.18	3.14	3.83	5.71	7.53	8.79	9.30	11.38	11.90	13.75
BCC-CSM-1-1, RCP 8.5	2.03	2.93	3.57	5.32	7.02	8.28	8.86	10.75	11.43	13.15
IPSL-CM5B-LR, RCP 4.5	1.26	1.81	2.21	3.29	4.34	5.57	6.32	7.34	8.58	9.64
CNRM-CM5, RCP 4.5	2.24	3.22	3.93	5.86	7.73	9.28	9.98	12.02	12.83	14.76
BCC-CSM-1-1, RCP 4.5	0.90	1.29	1.57	2.35	3.10	4.07	4.74	5.44	6.66	7.39

Figure 10. Updated 2050 IDF Curves for 200-year Recurrence Precipitation at Grand Rapids, MI

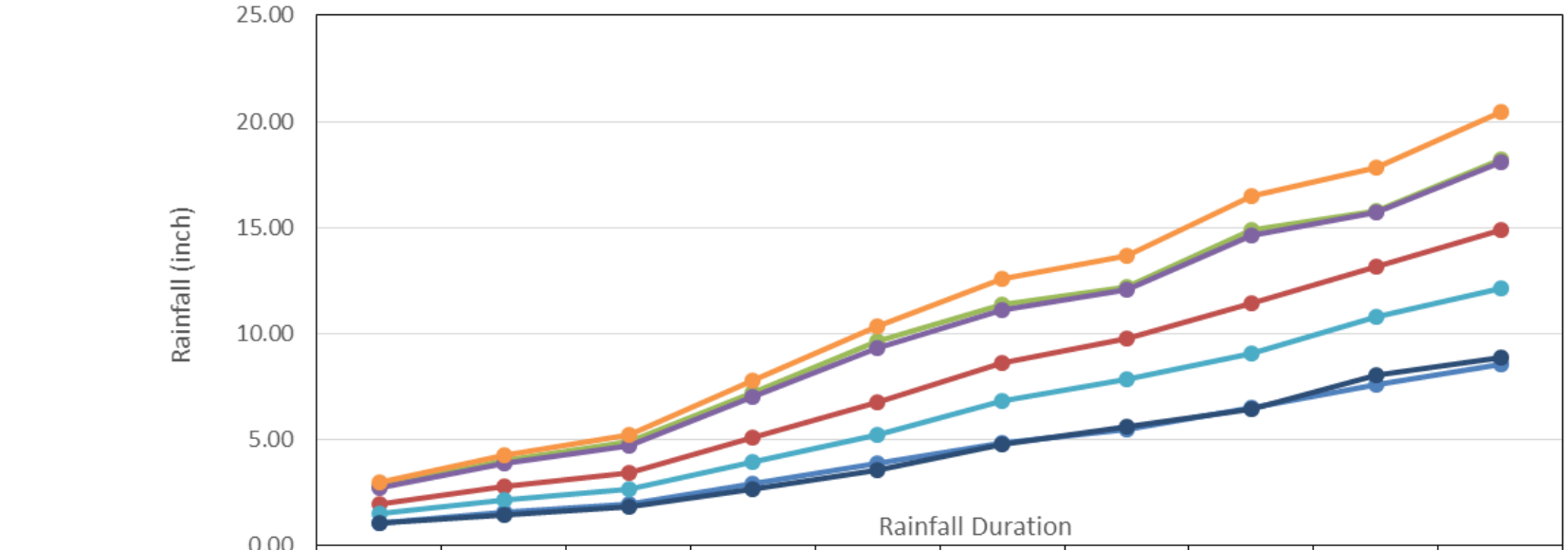

	5-min	10-min	15-min	30-min	1-hr	2-hr	3-hr	6-hr	12-hr	24-hr
NOAA Atlas 14	1.08	1.59	1.94	2.88	3.86	4.84	5.45	6.51	7.55	8.51
MIROC5, RCP8.5	1.94	2.79	3.41	5.05	6.72	8.61	9.76	11.39	13.18	14.87
CNRM-CM5, RCP 8.5	2.78	3.99	4.87	7.23	9.61	11.36	12.18	14.89	15.78	18.20
BCC-CSM-1-1, RCP 8.5	2.69	3.87	4.72	7.00	9.31	11.13	12.05	14.61	15.73	18.06
IPSL-CM5B-LR, RCP 4.5	1.50	2.16	2.64	3.91	5.20	6.80	7.84	9.06	10.80	12.10
CNRM-CM5, RCP 4.5	2.98	4.28	5.22	7.75	10.31	12.55	13.67	16.45	17.80	20.44
BCC-CSM-1-1, RCP 4.5	1.02	1.47	1.79	2.65	3.53	4.74	5.62	6.40	8.02	8.86

Figure 11. Updated 2050 IDF Curves for 500-year Recurrence Precipitation at Grand Rapids, MI

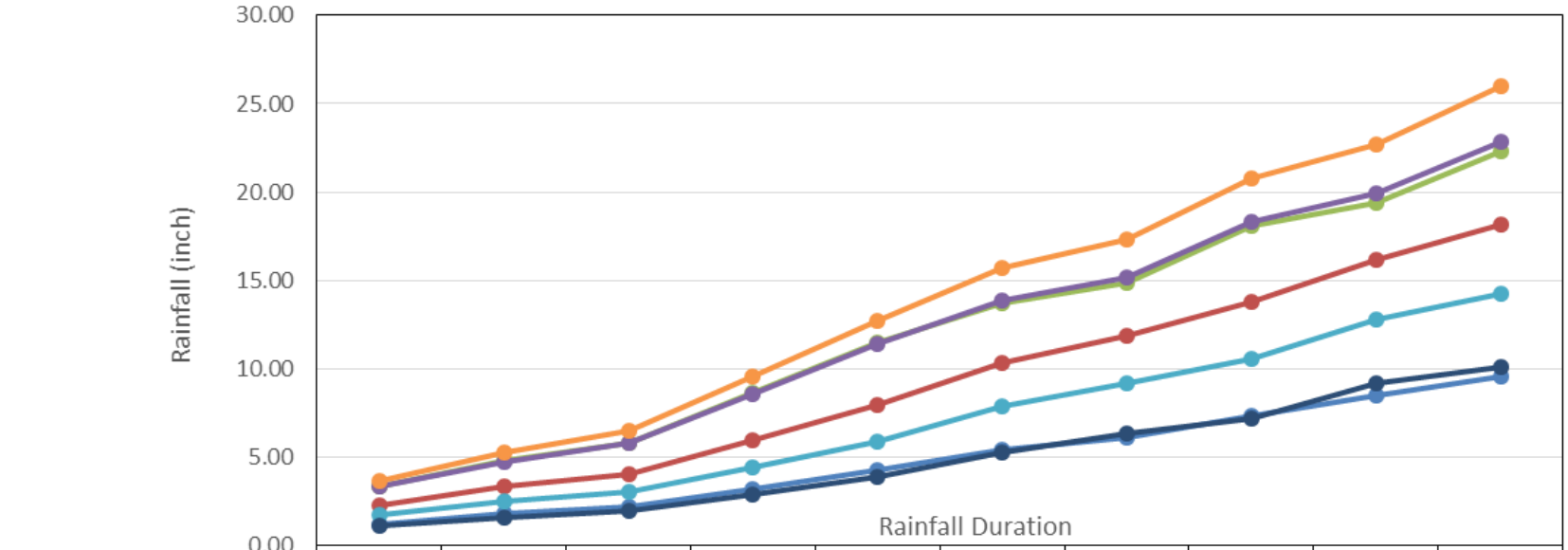

	5-min	10-min	15-min	30-min	1-hr	2-hr	3-hr	6-hr	12-hr	24-hr
NOAA Atlas 14	1.20	1.76	2.15	3.18	4.29	5.39	6.10	7.31	8.50	9.58
MIROC5, RCP8.5	2.29	3.30	4.02	5.97	7.94	10.31	11.85	13.76	16.15	18.17
CNRM-CM5, RCP 8.5	3.31	4.76	5.81	8.61	11.46	13.69	14.85	18.11	19.41	22.34
BCC-CSM-1-1, RCP 8.5	3.30	4.75	5.80	8.60	11.44	13.84	15.16	18.32	19.95	22.85
IPSL-CM5B-LR, RCP 4.5	1.71	2.46	2.99	4.44	5.91	7.84	9.17	10.54	12.76	14.24
CNRM-CM5, RCP 4.5	3.68	5.29	6.45	9.57	12.73	15.70	17.30	20.75	22.72	26.03
BCC-CSM-1-1, RCP 4.5	1.11	1.60	1.95	2.90	3.86	5.26	6.34	7.17	9.15	10.07

Figure 12. Updated 2050 IDF Curves for 1000-year Recurrence Precipitation at Grand Rapids, MI

4.2 IDF CURVES FOR 2085

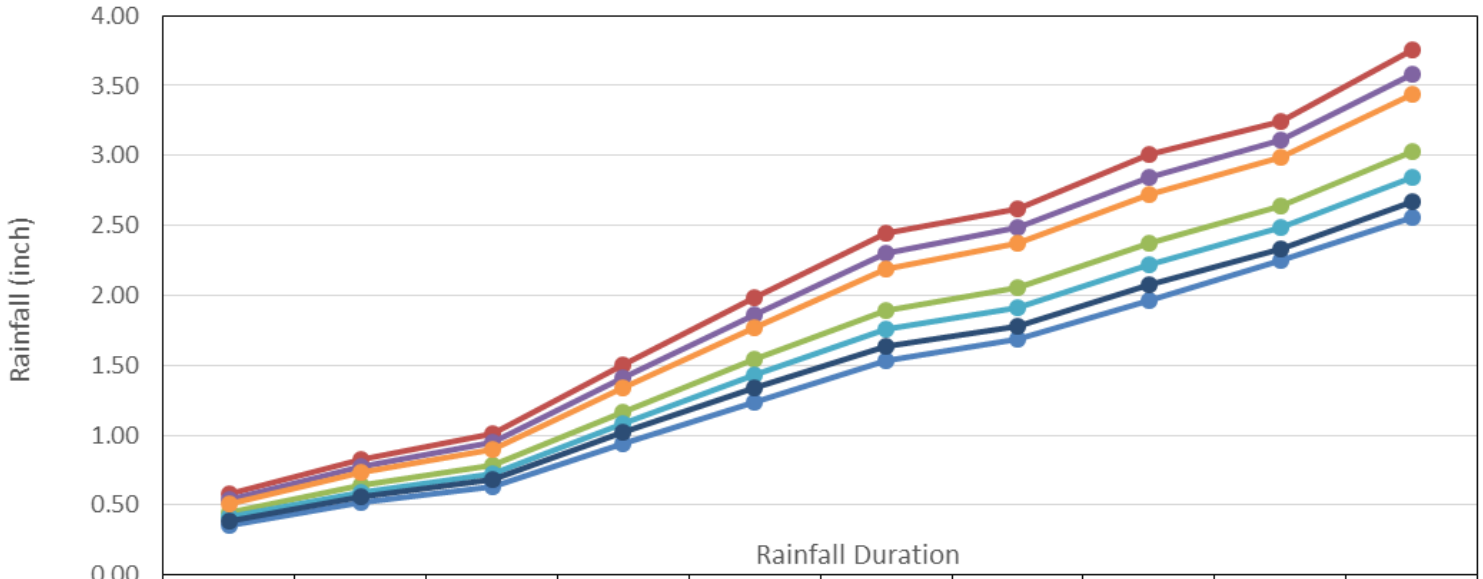

	5-min	10-min	15-min	30-min	1-hr	2-hr	3-hr	6-hr	12-hr	24-hr
NOAA Atlas 14	0.35	0.52	0.63	0.94	1.24	1.53	1.69	1.96	2.25	2.56
MIROC5, RCP8.5	0.58	0.83	1.01	1.51	1.99	2.44	2.62	3.01	3.24	3.75
CNRM-CM5, RCP 8.5	0.45	0.64	0.78	1.17	1.54	1.89	2.06	2.38	2.64	3.03
BCC-CSM-1-1, RCP 8.5	0.54	0.78	0.95	1.41	1.86	2.30	2.49	2.85	3.11	3.58
IPSL-CM5B-LR, RCP 4.5	0.41	0.60	0.73	1.08	1.43	1.76	1.91	2.22	2.48	2.85
CNRM-CM5, RCP 4.5	0.51	0.74	0.90	1.34	1.77	2.19	2.37	2.72	2.99	3.44
BCC-CSM-1-1, RCP 4.5	0.39	0.56	0.68	1.02	1.34	1.64	1.78	2.08	2.33	2.67

Figure 13. Updated 2085 IDF Curves for 2-year Recurrence Precipitation at Grand Rapids, MI

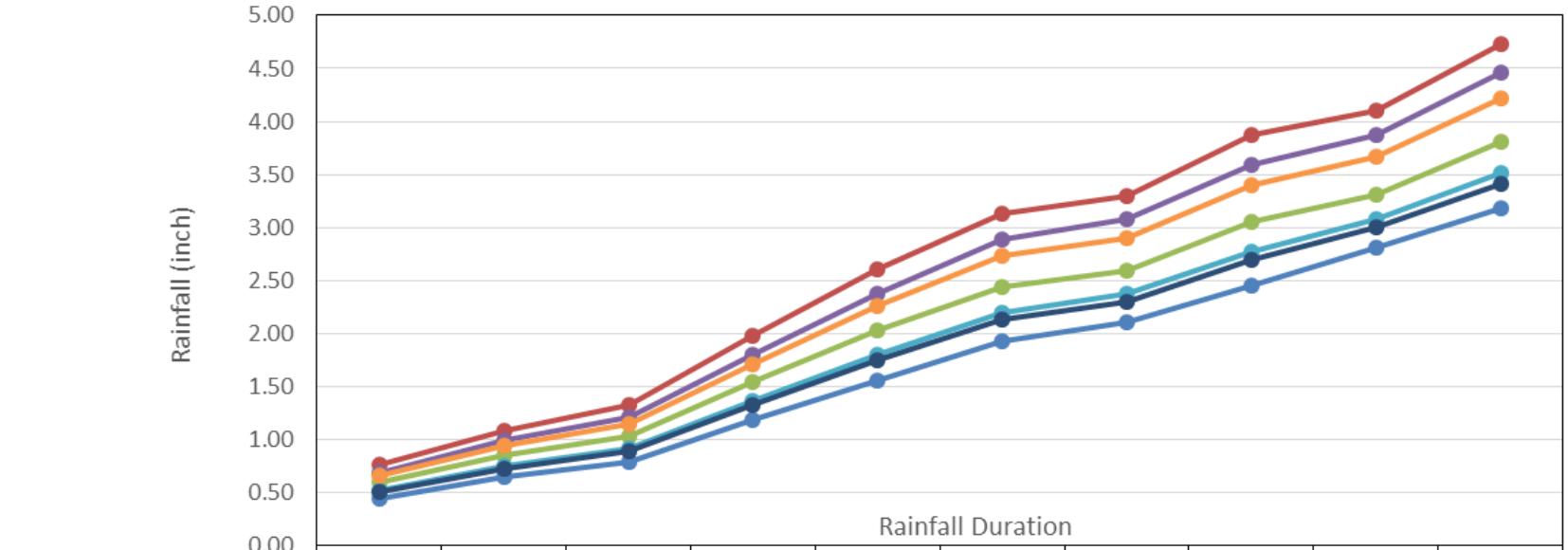

	5-min	10-min	15-min	30-min	1-hr	2-hr	3-hr	6-hr	12-hr	24-hr
NOAA Atlas 14	0.44	0.65	0.79	1.18	1.55	1.92	2.11	2.45	2.81	3.18
MIROC5, RCP8.5	0.75	1.09	1.32	1.98	2.61	3.13	3.30	3.87	4.10	4.73
CNRM-CM5, RCP 8.5	0.59	0.85	1.03	1.54	2.03	2.44	2.59	3.06	3.31	3.80
BCC-CSM-1-1, RCP 8.5	0.69	0.99	1.20	1.80	2.37	2.89	3.08	3.59	3.88	4.46
IPSL-CM5B-LR, RCP 4.5	0.52	0.75	0.91	1.36	1.80	2.20	2.37	2.77	3.08	3.52
CNRM-CM5, RCP 4.5	0.65	0.94	1.15	1.71	2.26	2.73	2.90	3.40	3.67	4.22
BCC-CSM-1-1, RCP 4.5	0.50	0.73	0.89	1.32	1.74	2.13	2.30	2.69	3.00	3.42

Figure 14. Updated 2085 IDF Curves for 5-year Recurrence Precipitation at Grand Rapids, MI

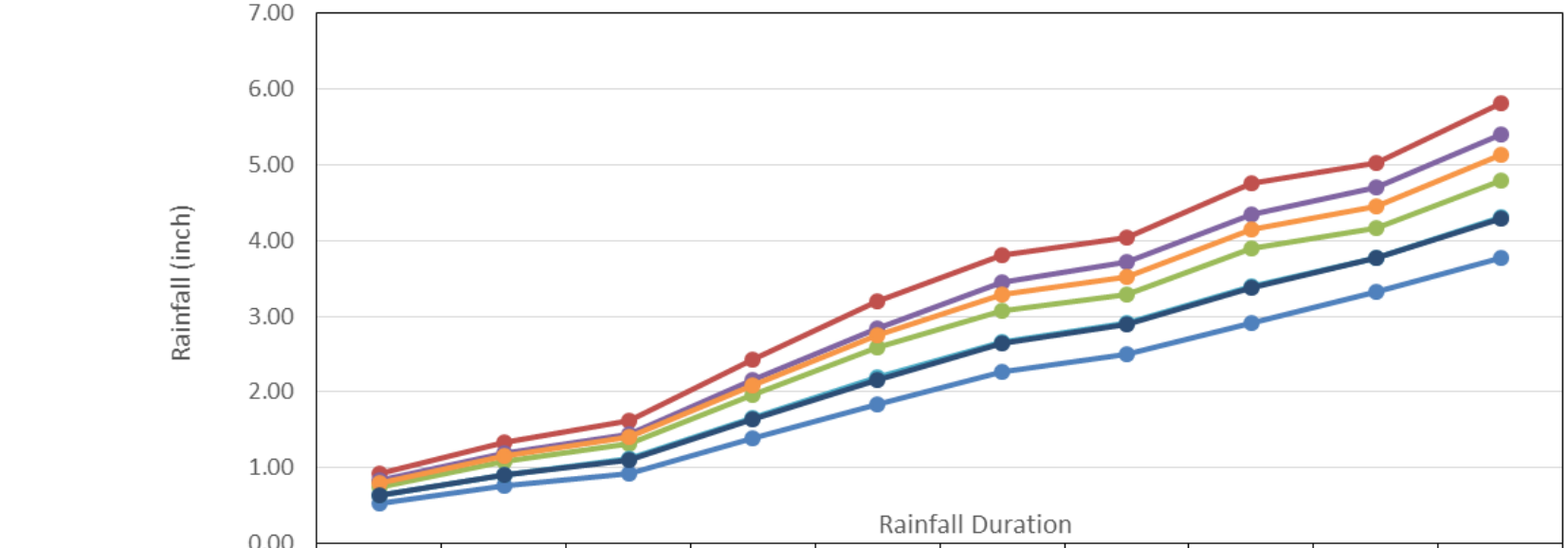

	5-min	10-min	15-min	30-min	1-hr	2-hr	3-hr	6-hr	12-hr	24-hr
NOAA Atlas 14	0.52	0.76	0.93	1.39	1.83	2.26	2.50	2.91	3.33	3.77
MIROC5, RCP8.5	0.93	1.33	1.63	2.43	3.20	3.81	4.04	4.77	5.03	5.81
CNRM-CM5, RCP 8.5	0.75	1.08	1.31	1.96	2.59	3.08	3.28	3.89	4.17	4.80
BCC-CSM-1-1, RCP 8.5	0.82	1.19	1.45	2.16	2.85	3.45	3.71	4.34	4.70	5.40
IPSL-CM5B-LR, RCP 4.5	0.63	0.91	1.11	1.66	2.19	2.67	2.91	3.40	3.78	4.31
CNRM-CM5, RCP 4.5	0.80	1.15	1.40	2.09	2.75	3.29	3.52	4.15	4.46	5.13
BCC-CSM-1-1, RCP 4.5	0.63	0.90	1.10	1.64	2.16	2.65	2.89	3.37	3.77	4.29

Figure 15. Updated 2085 IDF Curves for 10-year Recurrence Precipitation at Grand Rapids, MI

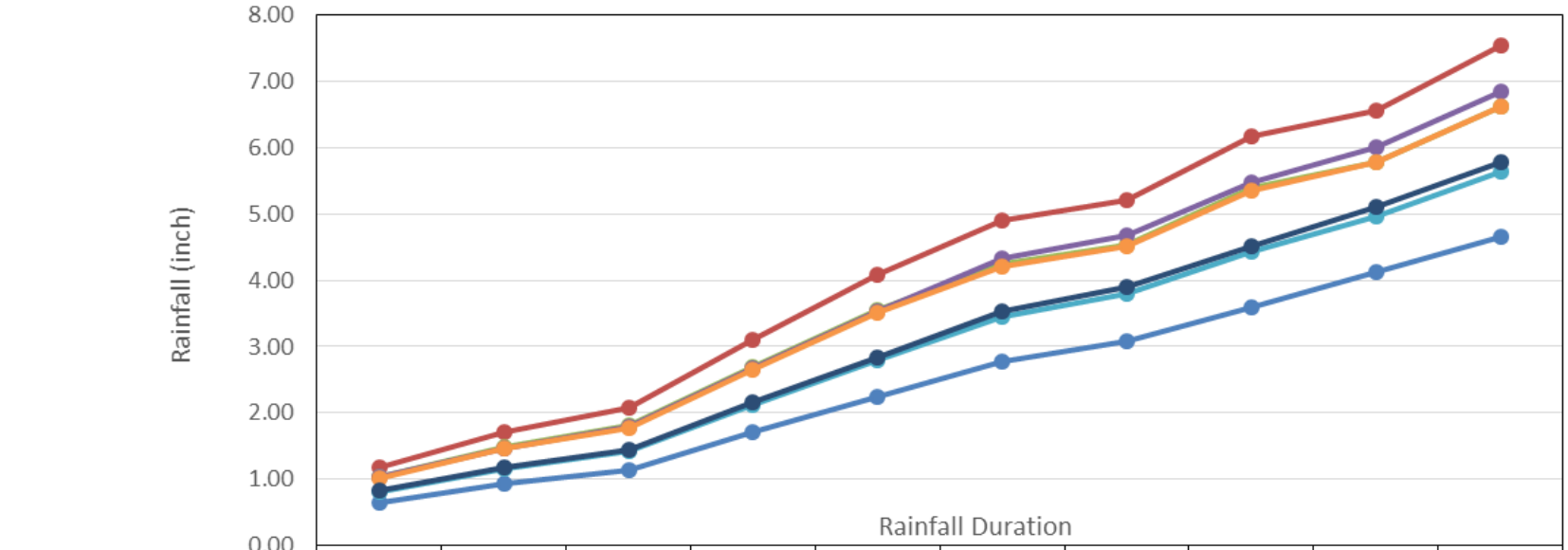

	5-min	10-min	15-min	30-min	1-hr	2-hr	3-hr	6-hr	12-hr	24-hr
NOAA Atlas 14	0.64	0.93	1.14	1.70	2.24	2.78	3.08	3.60	4.13	4.66
MIROC5, RCP8.5	1.18	1.70	2.08	3.10	4.09	4.90	5.21	6.17	6.56	7.55
CNRM-CM5, RCP 8.5	1.03	1.48	1.80	2.69	3.55	4.25	4.54	5.39	5.78	6.63
BCC-CSM-1-1, RCP 8.5	1.02	1.47	1.80	2.68	3.53	4.33	4.69	5.49	6.00	6.86
IPSL-CM5B-LR, RCP 4.5	0.81	1.17	1.42	2.12	2.80	3.46	3.79	4.43	4.97	5.64
CNRM-CM5, RCP 4.5	1.01	1.46	1.78	2.66	3.50	4.22	4.52	5.35	5.78	6.62
BCC-CSM-1-1, RCP 4.5	0.82	1.18	1.44	2.15	2.84	3.54	3.90	4.52	5.11	5.79

Figure 16. Updated 2085 IDF Curves for 25-year Recurrence Precipitation at Grand Rapids, MI

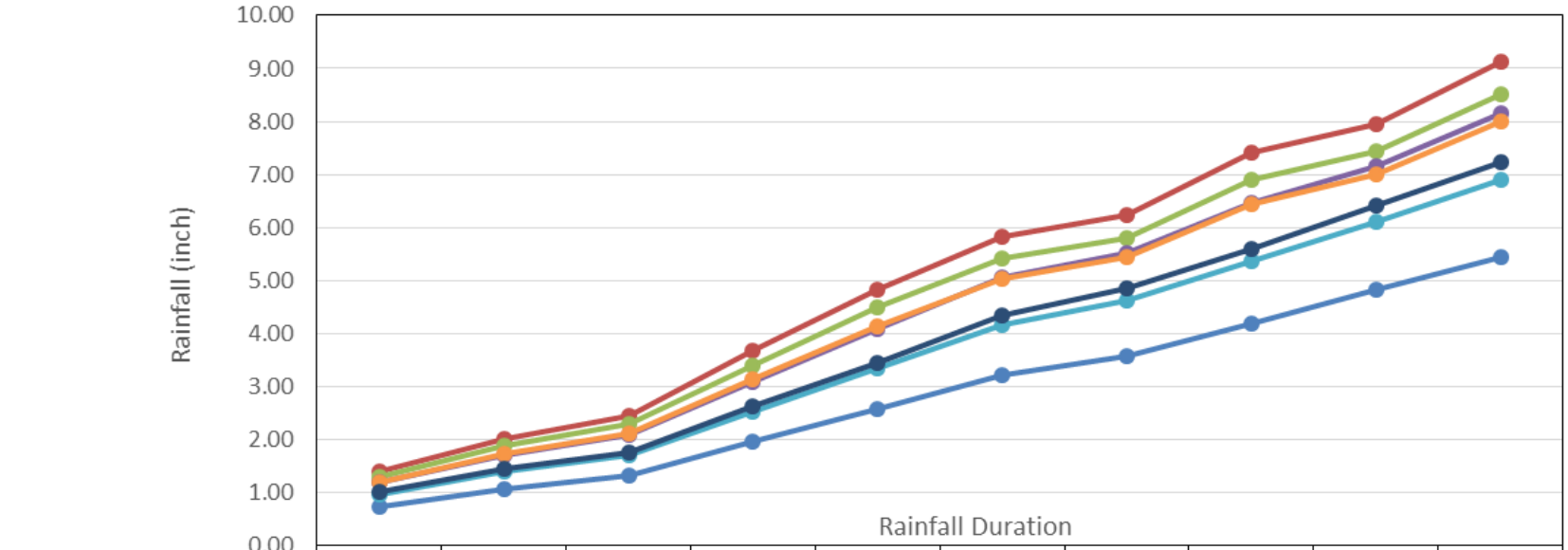

	5-min	10-min	15-min	30-min	1-hr	2-hr	3-hr	6-hr	12-hr	24-hr
NOAA Atlas 14	0.73	1.07	1.31	1.95	2.58	3.21	3.57	4.19	4.82	5.43
MIROC5, RCP8.5	1.40	2.01	2.45	3.66	4.83	5.82	6.25	7.41	7.95	9.12
CNRM-CM5, RCP 8.5	1.30	1.87	2.28	3.40	4.49	5.41	5.81	6.90	7.44	8.52
BCC-CSM-1-1, RCP 8.5	1.18	1.70	2.07	3.10	4.08	5.04	5.52	6.46	7.16	8.14
IPSL-CM5B-LR, RCP 4.5	0.96	1.39	1.69	2.52	3.33	4.16	4.61	5.37	6.10	6.89
CNRM-CM5, RCP 4.5	1.20	1.73	2.10	3.14	4.14	5.02	5.43	6.43	7.01	8.00
BCC-CSM-1-1, RCP 4.5	1.00	1.44	1.75	2.61	3.45	4.35	4.85	5.60	6.42	7.24

Figure 17. Updated 2085 IDF Curves for 50-year Recurrence Precipitation at Grand Rapids, MI

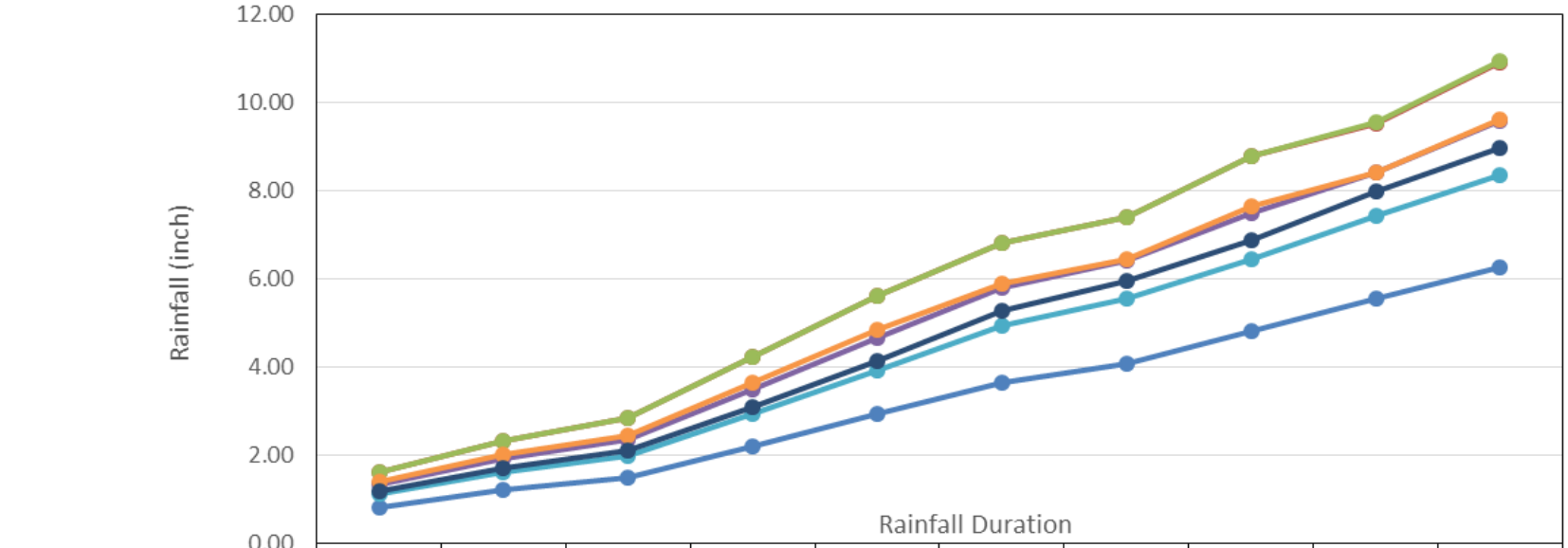

	5-min	10-min	15-min	30-min	1-hr	2-hr	3-hr	6-hr	12-hr	24-hr
NOAA Atlas 14	0.83	1.22	1.49	2.21	2.94	3.66	4.09	4.82	5.56	6.27
MIROC5, RCP8.5	1.62	2.33	2.84	4.22	5.61	6.82	7.39	8.77	9.52	10.91
CNRM-CM5, RCP 8.5	1.63	2.34	2.85	4.23	5.63	6.83	7.40	8.78	9.54	10.93
BCC-CSM-1-1, RCP 8.5	1.34	1.93	2.35	3.49	4.65	5.79	6.41	7.49	8.42	9.56
IPSL-CM5B-LR, RCP 4.5	1.13	1.63	1.98	2.94	3.91	4.94	5.55	6.43	7.41	8.36
CNRM-CM5, RCP 4.5	1.40	2.01	2.45	3.63	4.83	5.90	6.45	7.63	8.41	9.59
BCC-CSM-1-1, RCP 4.5	1.19	1.72	2.10	3.11	4.13	5.28	5.97	6.86	7.97	8.97

Figure 18. Updated 2085 IDF Curves for 100-year Recurrence Precipitation at Grand Rapids, MI

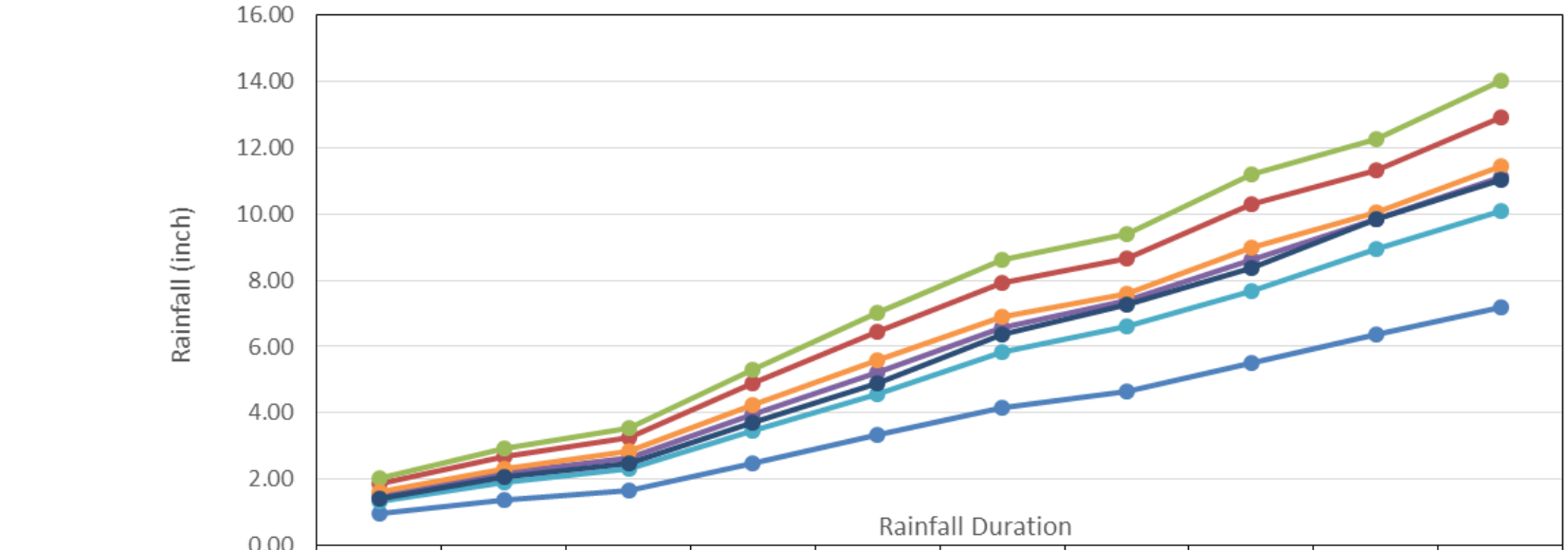

	5-min	10-min	15-min	30-min	1-hr	2-hr	3-hr	6-hr	12-hr	24-hr
NOAA Atlas 14	0.94	1.37	1.67	2.49	3.32	4.15	4.65	5.52	6.38	7.19
MIROC5, RCP8.5	1.86	2.68	3.27	4.88	6.44	7.92	8.67	10.31	11.33	12.94
CNRM-CM5, RCP 8.5	2.03	2.92	3.56	5.31	7.01	8.61	9.42	11.18	12.26	14.01
BCC-CSM-1-1, RCP 8.5	1.51	2.17	2.65	3.95	5.22	6.59	7.37	8.63	9.83	11.13
IPSL-CM5B-LR, RCP 4.5	1.32	1.90	2.31	3.45	4.55	5.84	6.63	7.68	8.97	10.08
CNRM-CM5, RCP 4.5	1.62	2.32	2.83	4.23	5.58	6.90	7.60	9.01	10.05	11.43
BCC-CSM-1-1, RCP 4.5	1.42	2.04	2.49	3.72	4.91	6.37	7.28	8.37	9.86	11.06

Figure 19. Updated 2085 IDF Curves for 200-year Recurrence Precipitation at Grand Rapids, MI

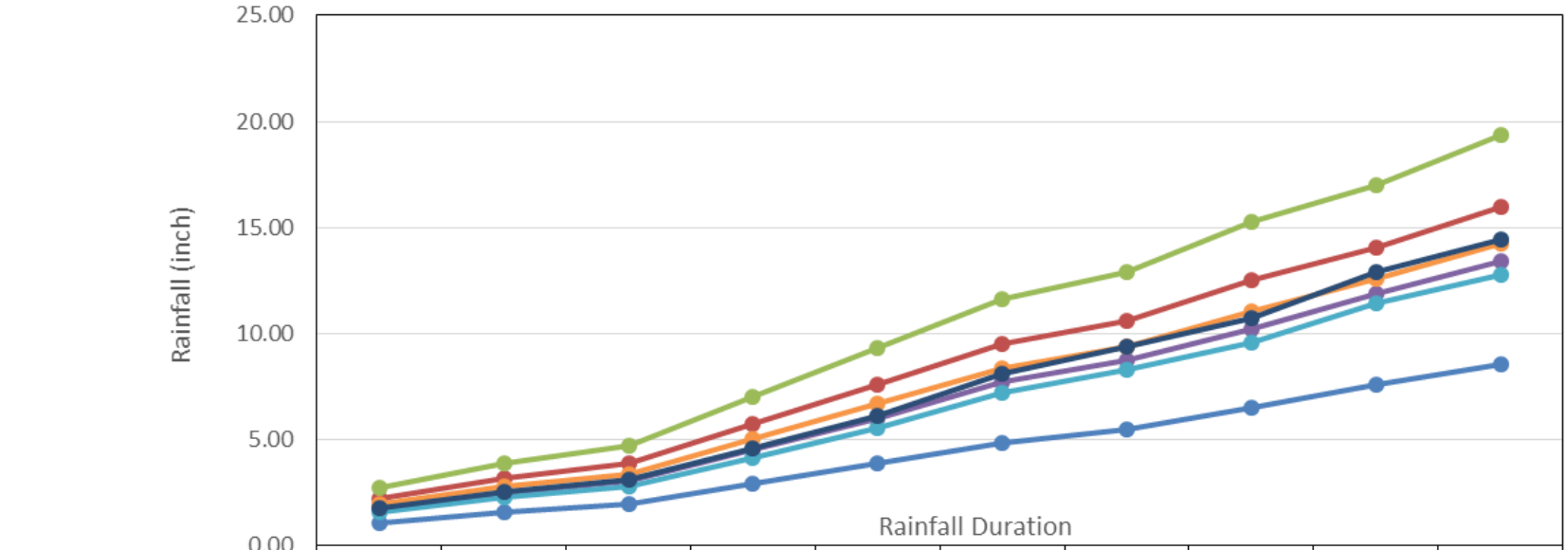

	5-min	10-min	15-min	30-min	1-hr	2-hr	3-hr	6-hr	12-hr	24-hr
NOAA Atlas 14	1.08	1.59	1.94	2.88	3.86	4.84	5.45	6.51	7.55	8.51
MIROC5, RCP8.5	2.20	3.16	3.85	5.72	7.61	9.51	10.57	12.54	14.04	15.98
CNRM-CM5, RCP 8.5	2.69	3.87	4.71	6.99	9.30	11.61	12.88	15.26	16.98	19.36
BCC-CSM-1-1, RCP 8.5	1.73	2.49	3.04	4.50	5.99	7.71	8.76	10.23	11.89	13.40
IPSL-CM5B-LR, RCP 4.5	1.59	2.29	2.79	4.14	5.50	7.20	8.30	9.58	11.40	12.77
CNRM-CM5, RCP 4.5	1.92	2.76	3.37	5.00	6.65	8.36	9.35	11.06	12.55	14.23
BCC-CSM-1-1, RCP 4.5	1.76	2.53	3.09	4.58	6.09	8.07	9.39	10.72	12.89	14.40

Figure 20. Updated 2085 IDF Curves for 500-year Recurrence Precipitation at Grand Rapids, MI

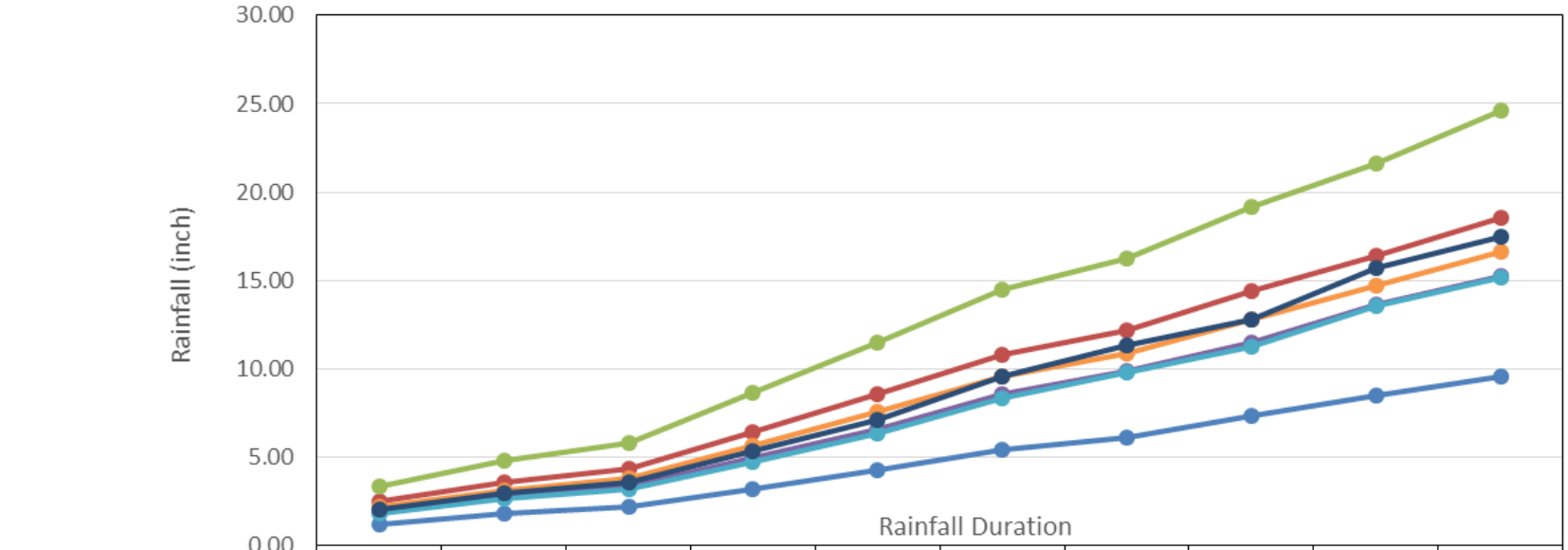

	5-min	10-min	15-min	30-min	1-hr	2-hr	3-hr	6-hr	12-hr	24-hr
NOAA Atlas 14	1.20	1.76	2.15	3.18	4.29	5.39	6.10	7.31	8.50	9.58
MIROC5, RCP8.5	2.46	3.55	4.32	6.41	8.53	10.81	12.17	14.39	16.36	18.56
CNRM-CM5, RCP 8.5	3.31	4.76	5.80	8.61	11.45	14.49	16.27	19.20	21.65	24.62
BCC-CSM-1-1, RCP 8.5	1.90	2.73	3.34	4.95	6.58	8.58	9.89	11.50	13.59	15.27
IPSL-CM5B-LR, RCP 4.5	1.82	2.62	3.19	4.73	6.29	8.36	9.77	11.22	13.56	15.14
CNRM-CM5, RCP 4.5	2.17	3.13	3.81	5.66	7.52	9.58	10.86	12.79	14.72	16.64
BCC-CSM-1-1, RCP 4.5	2.05	2.95	3.60	5.34	7.11	9.57	11.29	12.82	15.67	17.44

Figure 21. Updated 2085 IDF Curves for 1000-year Recurrence Precipitation at Grand Rapids, MI

(This page left intentionally blank.)

4.3 90TH PERCENTILE RAINFALL EVENT FOR 2050

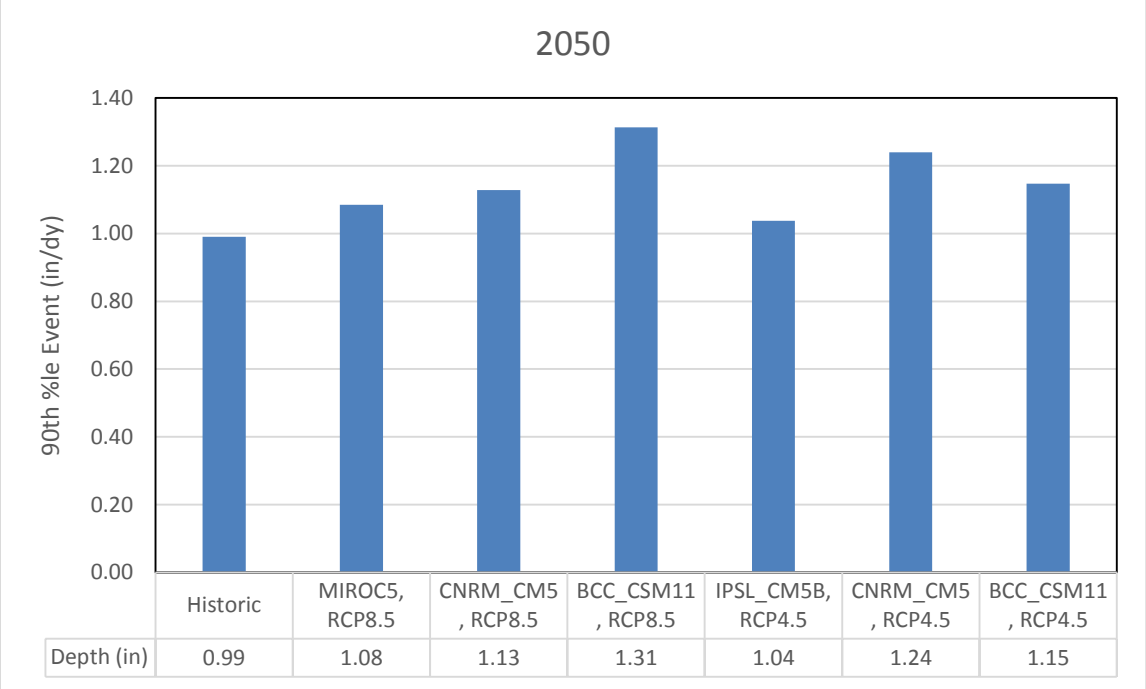

	Historic	MIROC5, RCP8.5	CNRM_CM5, RCP8.5	BCC_CSM11, RCP8.5	IPSL_CM5B, RCP4.5	CNRM_CM5, RCP4.5	BCC_CSM11, RCP4.5
Depth (in)	0.99	1.08	1.13	1.31	1.04	1.24	1.15

Figure 22. 90th Percentile Rainfall Event at Grand Rapids, MI for 2050

4.4 90TH PERCENTILE RAINFALL EVENT FOR 2085

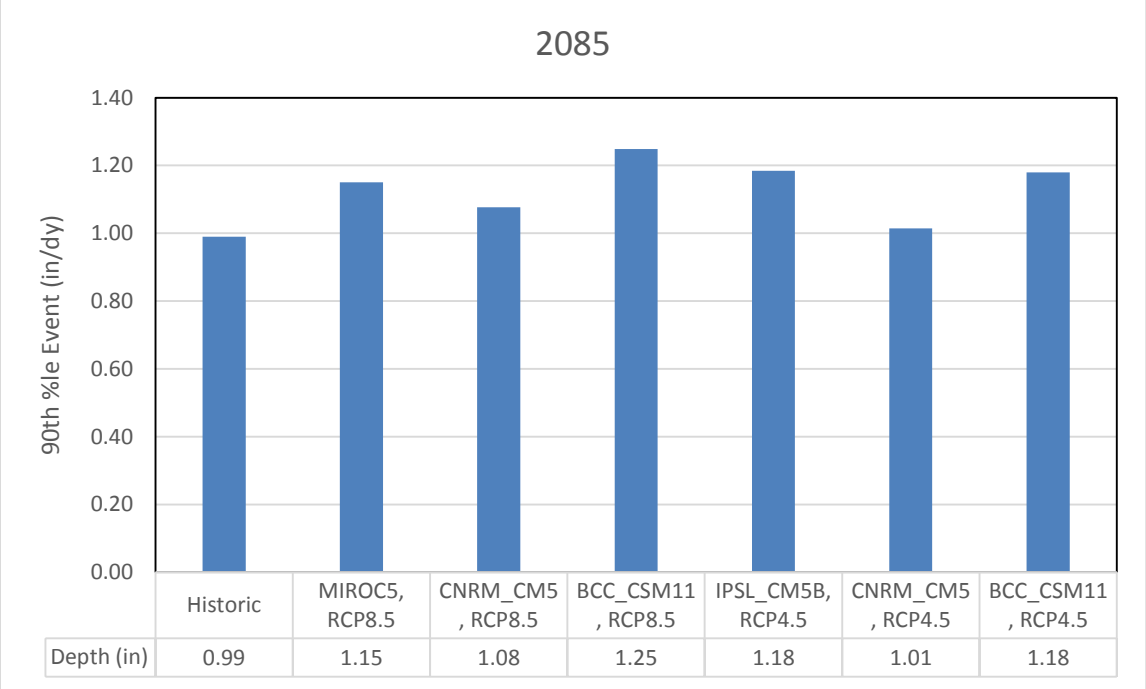

	Historic	MIROC5, RCP8.5	CNRM_CM5, RCP8.5	BCC_CSM11, RCP8.5	IPSL_CM5B, RCP4.5	CNRM_CM5, RCP4.5	BCC_CSM11, RCP4.5
Depth (in)	0.99	1.15	1.08	1.25	1.18	1.01	1.18

Figure 23. 90th percentile Rainfall Event at Grand Rapids, MI for 2085

(This page left intentionally blank.)

5 Discussion

Different global climate model predict a range of future precipitation regimes for Grand Rapids. Depending on the model, total rainfall may increase or decrease. It is clear, however, that warming air temperatures provide additional energy that is likely to increase the intensity of storm events.

For this study we selected a range of climate scenarios that span from the low to high end of future precipitation intensity as a way to identify the range of conditions to which adaptation may be needed. For 2050 conditions, one scenario (BCC-CSM-1-1, RCP 4.5) projects little change, and in some cases a decrease in rainfall intensity; however, the remaining scenarios show increases – up to 24% for the 24-hr 2-year event and up to 80% for the 24-hr 100-year event. The models that predict the largest increases in intensity for a given duration may well be over-estimates for future conditions, but this cannot be ascertained in advance. We believe it is reasonable to use the upper bounds of the estimated IDF curves for 2050 as protective design standards for future conditions. Additional changes are projected for 2085.

Results presented in Section 4 include recurrence intervals of up to 1000 years for consistency with NOAA Atlas 14. Estimates of extremely low probability events such as this are always subject to high levels of uncertainty. For future climate conditions this uncertainty is amplified by questions about the ability of the climate models to resolve such rare events. The longer-recurrence results are important in a qualitative sense to show how the risk of extreme flooding could increase, but it may be preferable to base quantitative design and management recommendations to results from the 100-year or lesser recurrence interval.

Table 2 provides a summary of commonly used rainfall events with and historical precipitation values for the corresponding events.

Table 2 Rainfall Summary Table

Event	Use	TP-40 1961 (inches)	Bulletin 71 1992 (inches)	Today – Atlas 14 (inches)	2050 (inches)	2085 (inches)
90%	Water Quality Treatment Volume	--	--	0.99	1.04 – 1.31	1.01 – 1.25
2-year 24-hour	Channel Protection	2.49	2.37	2.56	2.69 – 3.34	2.67 – 3.75
10-year 1-hour	Pipe Conveyance	1.81	1.65	1.83	1.81 – 3.01	2.16 – 3.20
25-year 24-hour	Local Flood Protection	4.23	4.45	4.66	4.67 – 7.06	5.64 - 7.55
100-year 24-hour	Local Flood Protection	4.99	6.15	6.27	6.39 – 11.06	8.36 – 10.93

(This page left intentionally blank.)

6 References

Abatzoglou, J.T. and T.J. Brown. 2012. A comparison of statistical downscaling methods suited for wildfire applications. *International Journal of Climatology*, 32: 772-780, doi:10.1002/joc.2312.

Allan, R.P., and B.J. Soden. 2008. Atmospheric warming and the amplification of precipitation extremes. *Science*, 321: 1481-1484, doi:10.1126/science.1160787.

Balkema, A.A., and L. de Haan. 1974. Residual life time at great age. *Annals of Probability*, 2(5): 792-804.

Hayhoe, K., D. Cayan, C.B. Field, P.C. Frumhoff, E.P. Maurer, N.L. Miller, S.C. Moser, S.H. Schneider, K.N. Cahill, E.E. Cleland, L. Dale, R. Drapek, R.M. Hanemann, L.S. Kalkstein, J. Lenihan, C.K. Lunch, R.P. Neilson, S.C. Sheridan, and J.H. Verville. 2004. Emissions pathways, climate change, and impacts on California. *Proceedings of the National Academy of Sciences of the U.S.A.*, 101: 12,422-12,427, doi:10.1073/pnas.0404500101.

Hosking, J.R.M., and J.R. Wallis. 1997. *Regional Frequency Analysis, an Approach Based on L-Moments*. Cambridge University Press

IPCC. 2007. Climate Change 2007: The Physical Science Basis. Contribution of Working Group I to the Fourth Assessment Report of the Intergovernmental Panel on Climate Change. [Solomon, S., Qin, D., Manning, M., Chen, Z., Marquis, M., Averyt, K.B., Tignor, M., and Miller H.L (eds.)]. Cambridge University Press, Cambridge, UK. http://www.ipcc.ch/publications_and_data/ar4/wg1/en/contents.html.

IPCC. 2013. Climate Change 2013: The Physical Science Basis. Contribution of Working Group I to the Fifth Assessment Report of the Intergovernmental Panel on Climate Change [Stocker, T.F., D. Qin, G.-K. Plattner, M. Tignor, S.K. Allen, J. Boschung, A. Nauels, Y. Xia, V. Bex and P.M. Midgley (eds.)]. Cambridge University Press, Cambridge, UK. http://www.ipcc.ch/report/ar5/wg1/.

Li, H., J. Sheffield, and E. F. Wood. 2010. Bias correction of monthly precipitation and temperature fields from Intergovernmental Panel on Climate Change AR4 models using equidistant quantile matching. *Journal of Geophysical Research: Atmospheres*, 115: D10101, doi:10.1029/2009JD012882.

Mehran, A., A. AghaKouchak, and T.J. Phillips. 2014. Evaluation of CMIP5 continental precipitation simulations relative to satellite-based gauge-adjusted observations. *Journal of Geophysical Research: Atmospheres,* 119: 1695-1707, doi:10.1002/2013JD021152.

Milly, P.C.D., J. Betancourt, M. Falkenmark, R.M. Hirsch, Z.W. Kundzewicz, D.P. Lettenmaier, and R.J. Stouffer. 2008. Stationarity is dead: Whither water management? *Science*, 319: 573-574, doi:10.1126/science.1151915.

Mote, P., L. Brekke, P.B. Duffy, and E. Maurer. 2011. Guidelines for constructing climate scenarios. *EOS, Transactions of the American Geophysical Union*, 92(31): 257-258.

Panofsky, H.A. and G.W. Brier. 1968. *Some Applications of Statistics to Meteorology*. Pennsylvania State University, University Park, PA

Patte, D. 2014. Climate Trends and Projections – A Guide to Information and References. U.S. Fish and Wildlife Service Pacific Region.

Pryor, S.C., D. Scavia, C. Downer, M. Gaden, L. Iverson, R. Nordstrom, J. Patz, and G.P. Robertson. 2014. Chapter 18, Midwest, pp. 418-440 in *Climate Change Impacts in the United State: The Third National Climate Assessment* [J.M. Melillo, T.C. Richmond, and G.W. Yohe, eds.] U.S. Global Change Research Program, doi:10.7930/J0J1012N. http://nca2014.globalchange.gov/report/regions/midwest.

Pryor, S.C., R.J. Barthelmie, and J.T. Schoof. 2013. High-resolution projections of climate impacts for the Midwestern USA. *Climate Research*, 56:61-79, doi:10.3354/cr01143.

Perica, S., D. Martin, S. Pavlovic, I. Roy, M. St. Laurent, C. Trypaluk, D. Unruh, M. Yekta, and G. Bonnin. 2013. Precipitation-Frequency Atlas of the United States. NOAA Atlas No. 14, Volume 8 Version 2.0: Midwestern States (Colorado, Iowa, Kansas, Michigan, Minnesota, Missouri, Nebraska, North Dakota, Oklahoma, South Dakota, Wisconsin). National Oceanic and Atmospheric Administration, Silver Spring, MD. http://www.nws.noaa.gov/oh/hdsc/currentpf.htm.

Pickands, J. III. 1975. Statistical inference using extreme order statistics. *Annals of Statistics*, 3(1): 119-131.

Serinaldi, F., and C.G. Kilsby. 2014. Rainfall extremes: Toward reconciliation after the battle of distributions. *Water Resources Research*, 50: 336-352, doi:10.1102/2013WR014211.

Sillmann, J., .V.V. Kharin, F.W. Zwiers, X. Zhang, and D. Bronaugh. 2013a. Climate extremes indices in the CMIP5 multi-model ensemble. Part 1: Model evaluation in the present climate. *Journal of Geophysical Research*, 118: 1716-1733, doi:10.1002/jgrd.50203.

Sillmann, J., .V.V. Kharin, F.W. Zwiers, X. Zhang, and D. Bronaugh. 2013b. Climate extremes indices in the CMIP5 multi-model ensemble. Part 1: Future projections. *Journal of Geophysical Research*, 118: 2473-2493, doi:10.1002/jgrd.50188.

Srivastav, R.K., A. Schardong, and S. P. Simonovic. 2014a. Equidistance quantile matching method for updating IDF Curves under climate change. *Water Resources Management*, doi:10.1007/s11269-014-0626-y.

Srivastav, R.K., A. Schardong, and S.P. Simonovic. 2014b. Computerized Tool for the Development of Intensity-Duration-Frequency Curves under a Changing Climate. Water Resources Research Report 089, University of Western Ontario, Dept. of Civil and Environmental Engineering, London, Ontario.

Toreti, A., P. Naveau, M. Zampieri, A. Schindler, E. Scoccimarro, E. Xoplaki, H.A. Dijkstra, S. Gualdi, and J. Luterbacher. 2013. Projections of global changes in precipitation extremes from Coupled Model Intercomparison Project Phase 5 models. *Geophysical Research Letters*, 40: 4887-4892, doi:10.1002/grl.50940.

Wigley, T. 2008. MAGICC/SCENGEN 5.3: User Manual (version 2). National Center for Atmospheric Research, Boulder, CO. http://www.cgd.ucar.edu/cas/wigley/magicc/UserMan5.3.v2.pdf.

WMEAC. 2013. Grand Rapids Climate Resiliency Report. Prepared for City of Grand Rapids Commission by Western Michigan Environmental Action Council, Grand Rapids, MI.